Development of an electrochemical (bio)sensor for quantification of cardiac biomarkers using molecular imprinting technology

Ana Teresa Gonçalves e Silva
Master's degree in Chemistry
Department of Chemistry and Biochemistry
2023

Supervisor
Dr. José Adolfo Oliveira Ribeiro, Researcher, CIQUP/DQB/FCUP

Co-Supervisor
Prof. Dr. Carlos Manuel de Melo Pereira, Professor, CIQUP/DQB/FCUP
Prof. Dr. Hélder Almeida Santos, Professor, BME/UMCG, NL

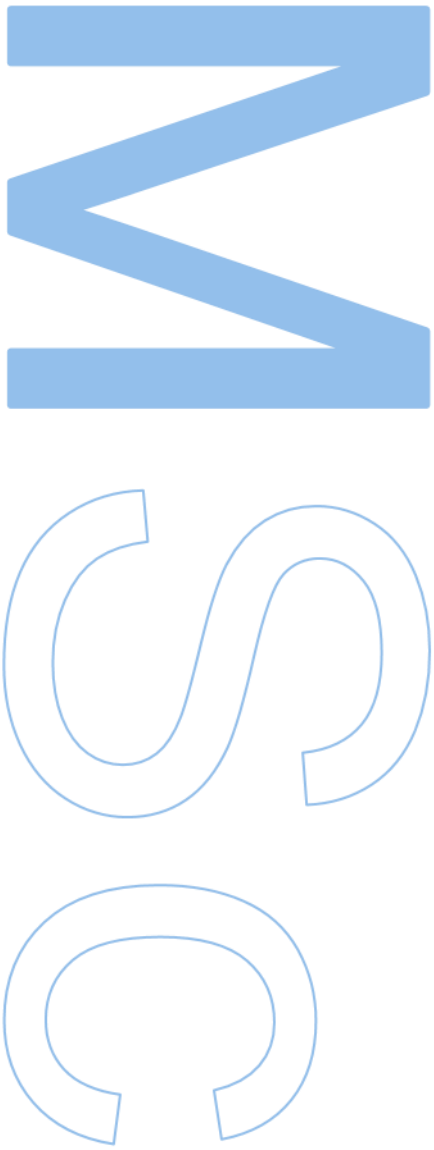


university of
groningen


UMCG


U.PORTO
FACULDADE DE CIÊNCIAS
UNIVERSIDADE DO PORTO

Agradecimentos

Em primeiro lugar, quero agradecer ao meu orientador, Doutor José Ribeiro, por todo o acompanhamento ao longo deste ano, por toda a disponibilidade, partilha de conhecimento, apoio e paciência.

Ao Professor Carlos Pereira, obrigada por todo o apoio e ensinamentos que me transmitiu ao longo destes anos.

Ao Professor Hélder Santos, obrigada por me receber tão bem no seu laboratório e por todo o apoio durante a minha estadia. À Raquel, por me ter acompanhado diariamente durante o meu tempo no Santos' Lab.

Quero agradecer ao Centro de Investigação em Química da Universidade do Porto (CIQUP), ao Santos' Lab (Países Baixos) e a todos os respetivos investigagadores pelo acolhimento e simpatia.

Quero também agradecer à Fundação para a Ciência e Tecnologia (FCT) o financiamento do projeto "MyTag – Universal environmental monitoring devices based on Intelligent scattering analysis enhanced by molecular Imprinted Tags" – PTDC/EEI-EEE/4832/2021.

Ao programa Erasmus+ Estágios, por ajudar na mobilidade ao Centro Universitário Médico de Groningen (UMCG, Países Baixos). Foram 3 meses muito enriquecedores, tanto a nível pessoal como profissional.

A quem me fez companhia e me apoiou durante o meu período no estrangeiro, à Maria Lobita, Soraia, Toni, Gabriela, Catarina e Maria Domingues. O vosso apoio foi indispensável.

Um especial obrigado à Patrícia, por toda a ajuda, paciência e conversas. Sem o teu apoio, este ano teria sido muito mais complicado. À Diana, pela amizade e por todos os momentos de descontração.

Ao meu namorado Ricardo, por todo o amor, paciência e motivação. Obrigada por celebrares todas as minhas vitórias como se fossem tuas.

Aos meus pais e ao meu irmão, por sempre me apoiarem em todos os meus desafios e nunca me deixarem sozinha. Obrigada por acreditarem em mim, mesmo quando eu não acredito.

Resumo

As doenças cardiovasculares são a maior causa de mortes mundialmente, tornando o diagnóstico precoce destas doenças muito importante para o seu tratamento eficiente, melhorando a taxa de sobrevivência e/ou permitindo uma melhor qualidade de vida dos pacientes. Neste contexto, o desenvolvimento de biossensores de baixo custo e portáteis com um *design* inovador e incorporando novos materiais "inteligentes" (como polímeros e nanomateriais) tem atraído grande interesse de pesquisa dentro da comunidade científica.

Este trabalho teve como objetivo desenvolver um biossensor amperométrico, integrando um recetor de filme de polímero molecularmente impresso (MIP), preparado por eletropolimerização de dopamina (DA) para quantificação seletiva do péptido natriurético atrial (ANP) tanto como biomarcador e agente terapêutico para doenças cardiovasculares. Elétrodos impressos de ouro (AuSPEs) foram utilizados como plataforma de deteção miniaturizada e com elevado custo-benefício para diagnóstico da doença no ponto cuidado (POC), ou para monitorização *in vitro* da internalização celular de nanopartículas (NPs) de ANP como sistema de libertação controlada de fármacos.

Neste trabalho, DA foi escolhida monómero eletroativo para construir o filme MIP devido à sua elevada biocompatibilidade e natureza hidrofílica. A polimerização eletroquímica foi realizada utilizando a técnica de voltametria cíclica (CV), onde o número de ciclos de varrimento foi otimizado para controlar a espessura do filme do polímero.

Outras condições experimentais foram otimizadas, nomeadamente o procedimento de extração da molécula molde e a concentração do molde (razão molde:monómero), de forma a melhorar o desempenho do biossensor MIP. Neste trabalho, a construção do biossensor MIP, tampão acetato 0.05 mol L^{-1}, pH 4.5, contendo 5 % (m/v) SDS foi utilizada como solução de extração, durante a noite, sob agitação suave. 0.5 mg mL^{-1} de ANP foi utilizada como concentração de molde ótima e 6 ciclos de CV foram realizados durante a eletropolimerização, a uma velocidade de varrimento de 0.05 V s^{-1}.

Após otimização das condições experimentais, a construção do biossensor utilizando a abordagem da impressão do epítopo foi também testada. Contudo, uma má seleção do epítopo de ANP levou a uma fraca impressão do molde na matriz polimérica e, subsequentemente, um baixo desempenho do biossensor e habilidade para reconhecimento do ANP.

Caracterização eletroquímica da superfície do elétrodo foi realizada durante a construção do biossensor passo-por-passo, utilizando as técnicas de CV e voltametria de onda-quadrada (SWV). As medições eletroquímicas foram realizadas na presença do par ferrocianeto/ferricianeto como sistema de repórter redox. Para além disso, caracterizações de microscopia de força atómica (AFM) e de microscopia de varrimento de eletrões (SEM) foram realizadas para avaliar a morfologia da superfície do filme MIP.

Para realizar os estudos de deteção, a superfície MIP foi incubada com várias soluções padrão de ANP, seguida de medições de SWV na presença de uma sonda redox externa. O chamado "*gate effect*" em filmes MIP foi utilizada para questões de quantificação. O sinal medido (intensidade de corrente de pico) permitiu a obtenção de curvas de calibração, com uma resposta linear na gama de concentrações entre 1.0 μmol L^{-1} e 1.0 mmol L^{-1}, com uma sensiblidade de - 0.033 mA L μmol^{-1} $década^{-1}$ e um limite de deteção (LOD) < 1.0 μmol L^{-1}.

Os resultados experimentais foram também ajustados a modelos de isotérmica de adsorção, onde a isotérmica de Freundlich apresentou o melhor ajuste aos resultados do MIP aqui obtidos, com um valor de K_F de 0.14 L μmol^{-1} e de n_F de 3.93.

A seletividade do biossensor foi também testada utilizando albumina de soro bovino (BSA), vancomicina e mioglobina como interferentes. O biossensor mostrou resposta considerável em relação à BSA e mioglobina, provavelmente devido à sua adsorção não-específica à superfície do MIP. No entanto, este não foi um problema neste trabalho uma vez que estudos em amostras biológicas não foram realizados.

Relativamente à aplicabilidade do biossensor MIP, estudos preliminares foram realizados para avaliar a resposta do biossensor à ANP como agente terapêutico utilizando um sistema de libertação controlada de fármacos sintetizado no Santos' Lab, um grupo de investigação dos Países Baixos. O biossensor de filme MIP conseguiu distinguir NPs funcionalizadas com ANP de NPs não-funcionalizadas. Resultados promissores foram obtidos para a utilização deste tipo de biossensor em estudos de internalização celular como uma alternativa simples e elevado custo-benefício a técnicas convencionais, como a citometria de fluxo.

Palavras-chave: polímeros molecularmente impressos (MIPs), péptido natriurético atrial (ANP), biomarcador cardíaco, elétrodo impresso de ouro (AuSPE), biossensor, eletroquímico, eletropolimerização, dopamina

Abstract

Cardiovascular diseases are the major cause of death worldwide, making the early diagnosis of these diseases very important for its efficient treatment, enhancing survival rate and/or allowing a better quality of life for patients. In this context, the development of low-cost and portable biosensors with innovative design and incorporating new "smart" materials (such as polymers and nanomaterials) has attracted great research interest within the scientific community.

This work aimed to develop an amperometric biosensor, integrating a molecularly imprinted polymer (MIP) receptor film, prepared by electropolymerization of dopamine (DA) for selective quantification of atrial natriuretic peptide (ANP) as both biomarker and therapeutic agent for cardiovascular diseases. Gold screen-printed electrodes (AuSPEs) were used as miniaturized and cost-effective detection platforms for point-of-care (POC) disease diagnosis, or for *in vitro* monitoring of cellular uptake of ANP nanoparticles (NPs) as a targeted drug delivery system.

In this work, DA was selected as redox-active monomer to build the MIP film due to its high biocompatibility and hydrophilic nature. The electrochemical polymerization was performed by using the cyclic voltammetry (CV) technique, where the number of scan cycles was optimized to control the polymer film thickness.

Other experimental conditions were optimized, namely the template extraction procedure and template concentration (ratio template:monomer), to enhance the MIP-biosensor performance. In this work, for the MIP biosensor construction, acetate buffer 0.05 mol L^{-1}, pH 4.5, containing 5 % (w/v) SDS was used as extraction solution, overnight, under gentle agitation. ANP 0.5 mg mL^{-1} was used as optimal template concentration and 6 CV cycles were performed during electropolymerization, at a scan rate of 0.05 V s^{-1}.

After optimization of the experimental conditions, the construction of the biosensor using the epitope imprinting approach was also tested. However, the bad selection of the ANP epitope led to poor imprinting of the template on the polymeric matrix and, subsequently, to low biosensor performance and ability for ANP recognition.

Electrochemical characterization of the electrode surface was performed during the step-by-step biosensor construction, using CV and square-wave voltammetry (SWV)

techniques. The electrochemical measurements were performed in the presence of the couple ferrocyanide/ferricyanide as redox reporting system. Furthermore, atomic force microscopy (AFM) and scanning electron microscopy (SEM) characterizations were performed to assess the morphology of the MIP film surface.

To perform the detection studies, the MIP surface was incubated with various ANP standard solutions, followed by SWV measurements in the presence of an external redox probe. The so-called "gate effect" in MIP films was used for quantification purposes. The measured signal (peak current intensity) allowed to obtain the calibration curves, with a linear response in the concentration range from 1.0 μmol L^{-1} to 1.0 mmol L^{-1}, with a sensitivity of - 0.033 mA L μmol^{-1} $decade^{-1}$ and a limit of detection (LOD) < 1.0 μmol L^{-1}.

The experimental data was also fitted to adsorption isotherm models, where the Freundlich isotherm presented the best fit to the MIP results here obtained, with a K_F value of 0.14 L μmol^{-1} and n_F value of 3.93.

The selectivity of the biosensor was also tested using bovine serum albumin (BSA), vancomycin and myoglobin as interferents. The biosensor showed considerable response towards BSA and myoglobin, probably due to its non-specific adsorption to the MIP surface. However, this was not a problem in this work as studies in biological samples were not performed.

Relatively to the applicability of the MIP-biosensor, preliminary studies were carried out to evaluate the biosensor response to ANP as a therapeutic agent using a targeted drug delivery system synthesized in Santos' Lab, a research group from the Netherlands. The MIP film biosensor could distinguish NPs functionalized with ANP from non-functionalized NPs. Promising results were obtained for the use of this type of biosensor in cell uptake studies as a simple and cost-effective alternative to conventional techniques, such as flow cytometry.

Keywords: molecularly imprinted polymers (MIPs), atrial natriuretic peptide, cardiac biomarker, gold screen-printed electrode (AuSPE), biosensor, electrochemical, electropolymerization, dopamine

Table of contents

List of tables

List of figures

List of equations

List of abbreviations

AFM	Atomic force microscopy
ANP	Atrial natriuretic peptide
AuSPE	Gold screen-printed electrode
BNP	B-type natriuretic peptide
BSA	Bovine serum albumin
CEA	Carcino-embryonic antigen
CNP	C-type natriuretic peptide
CV	Cyclic voltammetry
DA	Dopamine
DNA	Desoxyribonucleic acid
EDC	1-ethyl-3-(3-dimethylaminopropyl)carbodiimide
ELISA	Enzyme-linked immunosorbent assay
EMIP	Epitope molecularly imprinted polymer
HCF	Hexacyanoferrate
IF	Imprinting factor
IJUP	*Investigação Jovem da Universidade do Porto*
IUPAC	International Union of Pure and Applied Chemistry
LOD	Limit of detection
MI	Molecular imprinting
MIP	Molecularly imprinted polymer
MR-proANP	Mid-region of prohormone of atrial natriuretic peptic
MW	Molecular weight
nanoMIPs	Molecularly imprinted polymer nanoparticles
NHS	N-hydroxysuccinimide
NIP	Non-imprinted polymer
NPs	Nanoparticles
NT-proANP	N-terminal prohormone of atrial natriuretic peptide
NT-proBNP	N-terminal prohormone of brain natriuretic peptide
PB	Phosphate buffer
pI	Isoelectric point
PLGA	Poly(lactic-co-glycolic acid)
PLGA-NPs	Poly(lactic-co-glycolic acid) nanoparticles

PLGA-NPs@ANP	Poly(lactic-co-glycolic acid) nanoparticles functionalized with atrial natriuretic peptide
POC	Point-of-care
preproANP	Pre-prohormone of atrial natriuretic peptide
proANP	Prohormone of atrial natriuretic peptide
RMS	Root mean square
RT	Room temperature
SAM	Self-assembled monolayer
SDS	Sodium dodecyl sulphate
SEM	Scanning electron microscopy
SPE	Screen-printed electrode
SWV	Square-wave voltammetry
UV-Vis	Ultraviolet-visible

1. Introduction

According to the World Health Organization, cardiovascular diseases, mainly heart attack and stroke, are the leading cause of death globally. The majority of these deaths take place in low and middle-income countries.[1] In this context, the detection of cardiovascular biomarkers is currently a powerful tool for the early and accurate disease diagnosis and prognosis.

Nowadays, the development of accessible, portable and sensitive biomedical devices for screening cardiac biomarkers at point-of-care (POC) can play a crucial role in the clinical setting for the early-stage diagnosis and the establishment of personalized treatment plans for patients.[2]

The field of biosensors for screening cardiovascular biomarkers is rapidly growing. Over recent years, a lot of different fast response, reliable and sensitive biosensors have been developed to detect a widespread number of biomarkers, as highlighted in recent literature reviews[3, 4]. A lot of different cardiac biomarkers are already established in clinical practice. For atherosclerotic coronary disease there are biomarkers like troponin T and troponin I. Biomarkers like atrial natriuretic peptide (ANP) and brain natriuretic peptide (BNP) are associated with heart failure.[5, 6]

ANP, the target biomolecule of study in this work, has a big relevance in cardiovascular diseases, not only as a biomarker but also for targeting in newer drug delivery systems.

Some biosensors have been developed for ANP detection in recent years. Nagai *et al.*[7] proposed a sandwich chemiluminescent immunoassay employing secondary enzyme-labelled antibodies for selective ANP measurement directly in plasma samples of rats and mice. In 2019, Lin *et al.*[8] made use of the great features of molecular imprinting (MI) technology to develop a MIP film on a quartz crystal microbalance (QCM) disk for ANP detection in buffer. The epitope imprinting approach was used in their work due to the complexity of the cystine ring.

In another work, and combining the advantages of MI and nanotechnology, Wang *et al.*[9] synthesized molecularly imprinted nanoparticles (MIP NPs, also known as nanoMIPs) using the epitope imprinting approach for the fluorescent detection of ANP in human plasma with high selectivity when compared to bovine serum albumin (BSA).

The scientific community is currently pursuing new therapeutics for cardiovascular disease. In this context, another possible use of ANP is to perform targeted drug release by the functionalization of drug carrier systems with this molecule to confer more specificity to the target entities, in this case, to deliver drugs to cardiac cells. Santos' Lab, a research group from W.J. Kolff Institute for Biomedical Engineering and Materials Science from the University Medical Centre of Groningen, in the Netherlands, led by Professor Hélder A. Santos, has been developing new nanosystems based on ANP for targeted drug delivery to cardiac cells[10-12]. To establish the efficiency of such systems, various assays can be performed, like cell uptake studies, where the percentage of drug carrier systems that enter the cell is evaluated as a function of time. To evaluate drug uptake efficiency, the flow cytometry technique is usually used.

A collaboration between CIQUP and Santos' Lab was established to develop a simple and low-cost electrochemical biosensor for the detection of ANP-based nanosystems, being a viable alternative to the flow cytometry technique. To accomplish the proposed collaborative work, a mobility of 3 months (from February to April) to the Santos' Lab research group was performed under the Erasmus+ program. During this period, knowledge of the synthesis and posterior functionalization of NPs was acquired, as well as in atomic force microscopy (AFM) and screening electron microscopy (SEM) techniques.

The incorporation of molecularly imprinted polymers (MIPs) as receptors in biosensors has increased over recent years as they can specifically bind to the target analyte, being more stable, less expensive and their production easier when compared to biological antibodies.[13]

Herewith, the aim of this work was to develop an amperometric biosensor incorporating a MIP receptor film, prepared by electropolymerization of dopamine in a screen-printed electrode, for selective quantification of ANP as both biomarker and therapeutic agent for cardiovascular diseases. **Figure 1** shows a representation of the MIP biosensor developed.

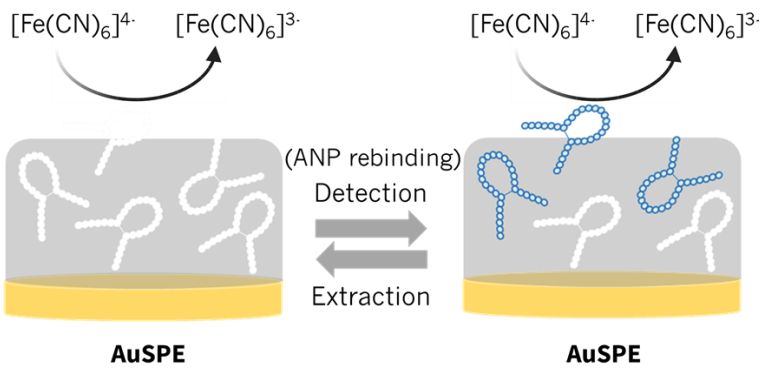

Figure 1 - Schematic representation of ANP MIP-based biosensor developed in this work.

The scientific outcomes from this work were:

- a literature review paper, entitled “Imprinted Hydrogel Nanoparticles for Protein Biosensing: A Review”, Silva, A. T.; Figueiredo, R.; Azenha, M.; Jorge, P. A. S.; Pereira, C. M.; Ribeiro, *ACS Sensors* 2023, DOI: 10.1021/acssensors.3c01010*;* that describes the preparation of biomimetic materials for protein detection[14];
- an oral presentation at the XV Scientific Mater of the master’s degree in Chemistry / FCUP entitled “Development of an electrochemical biosensor for ANP detection”, Silva, A. T.; Ribeiro, J. A.; Santos, H. A.; Pereira, C. M., 2023;
- a poster presentation with distinction at IJUP (*Investigação Jovem da Universidade do Porto*) entitled “Electrochemical biosensing of ANP using MIPs as receptors”, Silva, A. T.; Ribeiro, J. A.; Pereira, C. M., 2023;
- an oral presentation at the XXV Meeting of the Portuguese Electrochemical Society, entitled “Development of a molecularly imprinted polymer-based electrochemical sensor for ANP detection”, Silva, A. T.; Ribeiro, J. A.; Pereira, C. M., Coimbra, August 30th – September 1st, 2023.

To accomplish what was proposed, firstly a literature overview was done to better understand the state of the art and the scientific concepts related to this work.

2. Literature overview

2.1. Atrial natriuretic peptide

Natriuretic peptides are a family of endogenous hormones released by the heart being involved in the maintenance of cardiorenal homeostasis.[15, 16] There are three different groups of natriuretic peptides identified (**Figure 2**): atrial natriuretic peptide (ANP), B-type natriuretic peptide (BNP), and C-type natriuretic peptide (CNP).[17] In a myocardial infarction event, also known as a heart attack, vasoconstriction occurs and water retention increases in the body leading to atrial stretch (increased intracardiac pressure). This causes the release of ANP and BNP into the plasma as they present the function of regulating blood pressure by natriuresis and diuresis.[16, 18, 19]

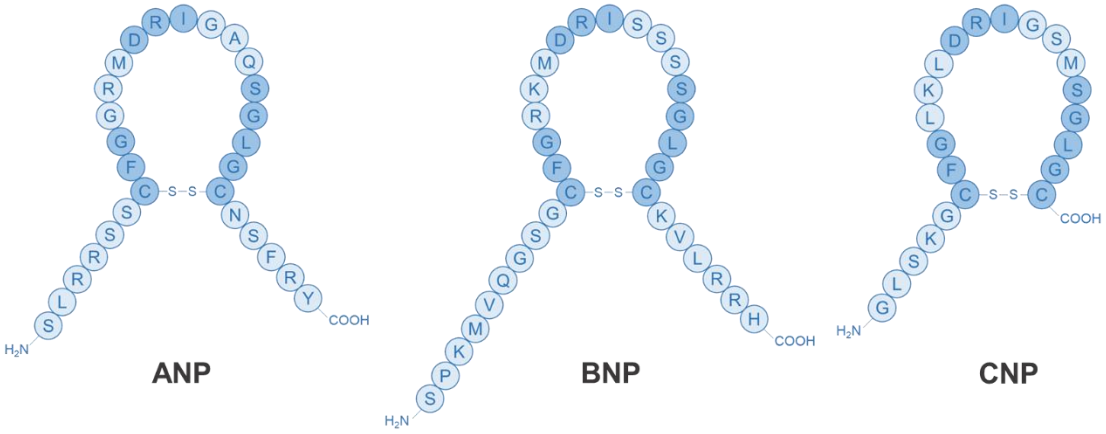

Figure 2 – Aminoacid sequence and structure of natriuretic peptides family. Conserved residues within the ring structures present a stronger blue colour.

ANP was first identified in 1981 by Bold e*t al.*[20] and its complete aminoacid sequence was discovered 3 years later by Kangawa *et al.*[21]. In healthy people, ANP is stored in cardiomyocytes in the atrium as its precursor pre-prohormone (preproANP, 151 aminoacids). After removal of the signal peptide by a peptidase, prohormone of ANP (proANP, 126 aminoacids) is obtained and stored in the granules in cardiomyocytes. Upon cell stimulation, by mechanical stretch for example, proANP is cleaved by corin protease, during exocytosis, releasing to the bloodstream two fragments: N-terminal proANP (NT-proANP, 98 aminoacids) and mature ANP (C-terminal peptide, 28 aminoacids) (see **Figure 3**). In patients with heart failure, the NT-proANP cleaved products are not only present in the plasma but also in the cardiomyocytes.[18, 22]

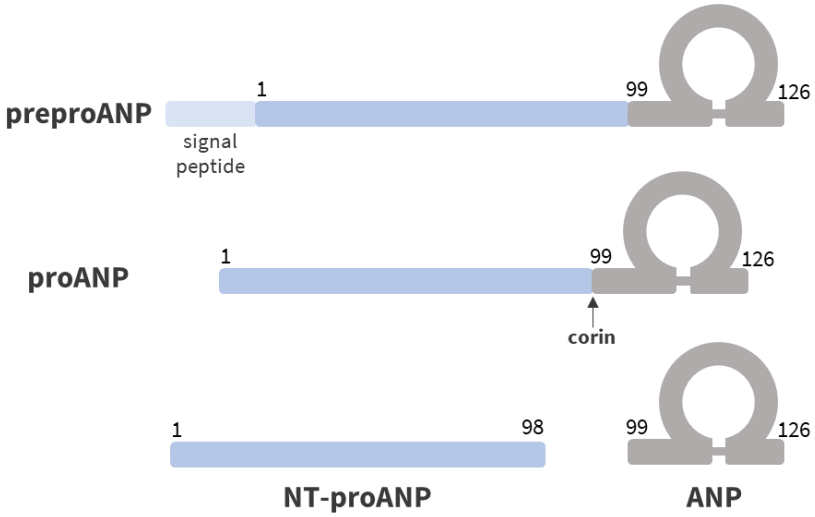

Figure 3 - Schematic representation of ANP processing: from preproANP to mature ANP.

According to the National Institute of Health Consortium, a biomarker is defined as a "*characteristic that is objectively measured and evaluated as an indicator of normal biological processes, pathogenic processes, or pharmacologic responses to a therapeutic intervention*".[23] Thus, an ideal biomarker should be specific to a disease condition and its normal and abnormal levels should be well-established (cut-off values).[5]

Although ANP is considered a cardiovascular disease biomarker under evaluation[5], it presents a short half-life in human plasma (approximately 2 minutes)[24, 25] which makes ANP detection in blood rather challenging, especially when compared to BNP (half-life of approximately 22 minutes) or even to the N-terminal prohormone of BNP (NT-proBNP, 120 minutes)[26]. Consequently, it is not surprising that only one immunoassay to detect proANP through its mid-region, also known as MR-proANP, is commercially available.[27] Still, the lack of reliable data about MR-proANP and the degradation of NT-proANP in 3 different fragments in human plasma, makes MR-proANP a less reliable biomarker when compared to BNP and/or NT-proBNP.[28, 29]

One of the reasons for the ANP's short half-life is its binding to natriuretic peptide receptors present in the cardiac cell membrane.[17] However, this well-known interaction was useful for researchers to develop new targeted drug delivery systems to treat cardiovascular diseases, by functionalizing the surface of drug-loaded nanoparticles (NPs) with ANP molecules, making them more prone to cross the cell membrane. Different nanosystems have already been synthesized for this purpose by Santos' Lab research group[10-12].

2.2. Biosensors

According to IUPAC (International Union of Pure and Applied Chemistry), a chemical sensor is "*a device that transforms chemical information, ranging from the concentration of a specific sample component to total composition analysis, into an analytically useful signal*".[30] A chemical sensor is composed of two main components: a (i) recognition system, also known as receptor, that will selectively recognize the target analyte, and a (ii) physico-chemical transducer, that converts the recognition event into a measurable signal, that is further processed and displayed. A biosensor is a chemical sensor integrating a biological receptor (see **Figure 4**).[31, 32]

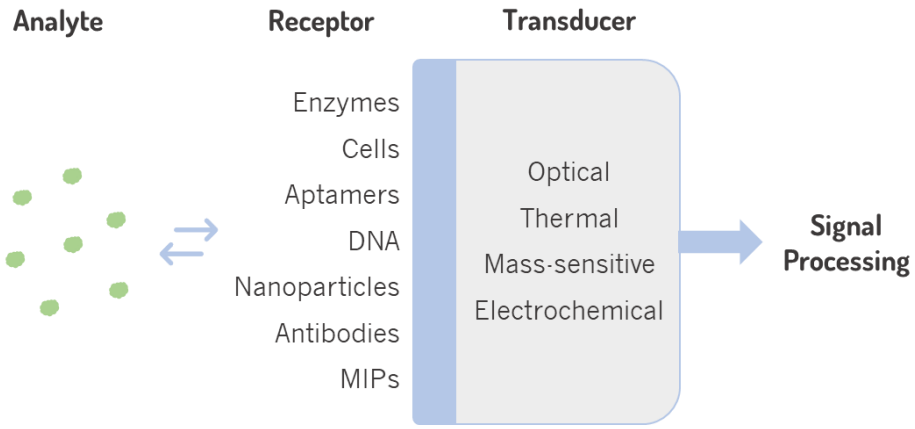

Figure 4 - Schematic representation of the components of a biosensor and its operation mode.

Biosensors can be classified according to the receptor used (i.e., enzyme – enzymatic sensor, oligonucleotide – genosensor, antibody - immunosensor, aptamer – aptasensor), the transduction mode in use (optical, thermal, mass-sensitive or electrochemical), or a mixture of the two (i.e. electrochemical immunosensor).[32]

Many biosensors developed to date for the sensing of different types of analytes are based on electrochemical transduction mode.[33, 34] These have been used in various relevant applications, such as disease diagnosis[35, 36], environmental analysis[37], and precision medicine[2].

The electrochemical methods present unique characteristics, such as high sensitivity, fast response time, and low-cost analysis, that have promoted an exponential increase in the development of new electrochemical biosensors over the past decade.[38] These methods can be divided into three categories: potentiometry, amperometry and impedance.[14]

Furthermore, the possibility of miniaturization of electrochemical devices, i.e., using screen-printed electrodes (SPEs) or paper-based devices[39], allowed the portability of this type of sensors for point-of-care (POC) analysis or *in situ* monitoring of the target analyte.[2, 40]

Over the last years, the interest in using biomimetic materials, such as molecularly imprinted polymers (MIPs), as synthetic receptors in (bio)sensors has exponentially increased due to their higher stability and lower production cost when compared to natural antibodies, making them very appealing for sensing applications.[13]

2.3. Molecularly imprinted polymers (MIPs)

2.3.1. The concept of Molecular Imprinting

Molecularly imprinted polymers (MIPs) are synthetic receptors that present high affinity and selectivity towards a specific molecule. The concept of molecular recognition was introduced in the 1930s and this technology has been evolving since then with the use of different preparation methods, such as surface imprinting, precipitation polymerization, and emulsion polymerization, among others, allowing the preparation of imprinted materials with different shapes and sizes.[14, 41] In addition, the MI technology has been applied for the recognition of different types of molecules, from small drugs and pesticides to peptides, proteins, virus, bacteria and even cells, increasing the interest and potential of this technology.[13, 14]

Generally speaking, the imprinting process of a template, usually the target analyte, involves the use of functional monomers that can establish specific molecular interactions with the template molecule, that in the presence of a cross-linker reagent constructs a 3D polymeric matrix around it. The subsequent removal of the template from the polymeric matrix leaves behind molecular cavities (binding sites) that are complementary to the template in terms of size, shape, and functional groups (see **Figure 5**).[13, 42]

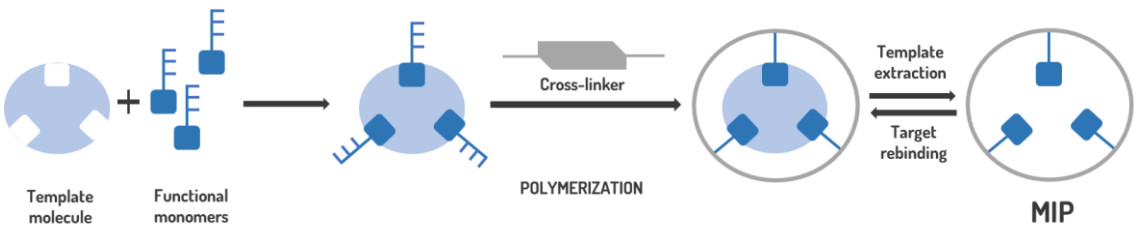

Figure 5 - Schematic representation of the MIP formation process.

2.3.2. MIPs as an alternative to natural antibodies for biosensing applications

MIPs, also known as “plastic antibodies”, have been widely used in various fields, including biosensing.[13] Natural antibodies present some unfavourable characteristics for their use in this field, such as high acquisition costs, restricted handling and storage conditions and instability in harsh environments. Thus, MIPs have been seen for the past years as a promising alternative.[13, 43] These biomimetic materials present recognition properties similar to natural antibodies but offer long-term stability and much lower production costs.[14] One major representative example of the increasing interest in this technology is the use of MIPs for protein biosensing. Various review papers have been published in the last years about this topic.[38, 42, 44-46]

2.3.3. Polydopamine MIP film prepared by electrochemical polymerization

For electrochemists, a simple and fast route for MIP synthesis is through surface electrochemical polymerization of a mixture of a redox-active monomer and the template molecule, resulting in a MIP film deposited on an electrode surface.[14, 38, 47] The thickness of the film can be easily controlled during the electropolymerization process by changing some parameters according to the electrochemical technique chosen to perform the electrosynthesis. For example, if chronoamperometry is used, the period of time that a certain potential is applied to the working electrode controls the film thickness. If cyclic voltammetry (CV) is chosen, the number of scan cycles performed can be adjusted to control the film thickness.[38, 48]

A variety of monomers have been used to perform MIP electropolymerization, such as aniline, pyrrole, scopoletin, and dopamine (DA), among others.[38, 47]

In this work, DA was chosen as monomer for MIP construction. DA presents two main functional groups, amino and phenolic groups, that allow the establishment of various molecular interactions (hydrogen bonding, electrostatic interactions, etc.) with other molecules and substrates.[49, 50] Since its discovery in 2007[51], polydopamine films became very relevant bioinspired materials for coating different substrates[52] that found many applications in biomedical science[53], regenerative medicine[54] and in the biosensing field[55, 56]. This polymer presents some advantages when compared to others, such as high biocompatibility and its hydrophilic nature, which can minimize non-specific adsorption to the sensing platforms.[55]

There are two main ways to prepare a polydopamine film. DA can undergo self-polymerization under alkaline conditions (pH > 7.5) or, given its redox properties, it can also be polymerized at the electrode surface by electrochemical methods to obtain a polydopamine film.[50]

Given its unique properties, the use of DA has been particularly promising to construct MIPs for analytical applications. Some works emerged in literature in the past years. Recently, in 2019, Qi *et al.*[57] reported the preparation of a microfluidic analytical device for the electrochemical detection of cancer biomarker carcino-embryonic antigen (CEA) in a clinical context. In 2020, Leibl *et al.*[58] prepared an electrochemical sensor for the detection of nitro-explosives in aqueous solutions. Meanwhile, in 2021, Roushani *et al.*[59] developed MIP electrochemical sensor for selective detection of pesticide Asulam. In these works, DA was electropolymerized by using CV to create a MIP receptor film layer on the electrode surface for selective detection of the respective targets.

2.3.4. Template extraction

An efficient template extraction from the polymeric matrix is a fundamental step in MIP formation since it can affect the MIP performance. A good extraction method should repress the interactions between the template molecule and the polymer, allowing effective template removal and leaving behind specific recognition sites for the target analyte.[60] On the other hand, the extraction solution should not affect the polymer, which could lead to the deformation of the binding sites and/or damage of the film.[46]

Over the years, several methods have been used for the template removal. Focusing on protein imprinting, the most commonly used strategy is the MIP submersion in acidic/basic aqueous solutions (acetic acid, oxalic acid, sodium hydroxide, etc.), containing or not surfactants (e.g. SDS). [46, 61] An alternative to the use of harsh solvents is the use of enzymatic methods, namely the proteolytic digestion using proteinase K or trypsin.[62]

2.3.5. Electrochemical analysis of non-redox active biomolecules

For MIP-based electrochemical biosensors, the typical approach to perform the detection of non-electroactive targets, such as peptides and proteins, is by performing indirect electrochemical measurement in the presence of an external redox probe.[38] This

electrochemical readout is based on the so-called “gate effect”, which is considered an electrode-electrolyte phenomenon.[63]

In MIP films, this effect results from the interaction of the polymer with the target analyte.[63] The simplest mechanism is the diffusion-controlled that can be explained with three different phenomena: (i) the MIP film contraction and expansion caused by target rebinding; (ii) the charge accumulation in the MIP film when they are used for the detection of charged analytes; (iii) the physical blocking of the binding cavities, at the MIP film, by target analyte molecules. In most of the cases, these changes decrease the diffusion rate of the redox probe through the MIP film to the electrode surface, translating in a lower measured electrochemical signal as function of target analyte concentration.[63]

2.3.6. Epitope imprinting

As stated before, there are various molecular imprinting techniques that can be used for protein imprinting, such as surface imprinting, precipitation polymerization, etc. These imprinting processes use the whole protein as template and create binding sites on the surface of a polymeric matrix.[64] However, this technique presents some challenges due to the complex and flexible structure of proteins, making difficult its extraction from the polymeric matrix.[65]

On the other hand, a straightforward strategy, compatible with the previously mentioned MIP synthesis routes, has been extensively used for protein imprinting, the epitope imprinting.[42] In this technique, only a fragment of the target protein, called epitope (approximately 10 aminoacids from the external structure of the protein), is used as template to prepare the MIPs.[65, 66] This last one can benefit the template extraction from the polymeric matrix and also decrease the production cost of the biosensor, due to the high cost of some proteins. After the epitope removal, the prepared MIP presents specific binding sites with recognition properties for the entire target protein.[14]

2.4. Electrochemical techniques

The electrochemistry field is in constant evolution to better understand and explain reactions that occur on the electrode surface. Furthermore, electrochemical techniques can be used in electroanalytical studies for rapid, simple and sensitive detection of chemically and biologically relevant (bio)molecules. The electrochemical techniques can

be divided in 4 categories: amperometric, that measures changes in the electric current; potentiometric, that measures changes in the potential; conductometric, where changes in the conductance are recorded and; impedimetric, that measures changes in the impedance of the system.[67]

In this work, two amperometric techniques, cyclic voltammetry (CV) and square-wave voltammetry (SWV), were used for the electrode surface characterization along the step-by-step construction of the MIP biosensor. To evaluate the biosensor performance in the detection studies, SWV was selected as quantification technique.

2.4.1. Cyclic voltammetry

CV is an electrochemical technique usually applied to investigate the reduction and oxidation processes of molecules. With a defined scan rate, a linear potential is applied on an electrode in function of time, from an initial value (E_{start}) until a switching potential predetermined (E_{λ}) where the direction of the scan is reversed (see **Figure 6-A**), while recording the current flow (see **Figure 6-B**).[68, 69] **Figure 6-A** shows the symmetry that characterizes the plot of the linear potential applied on the electrode in function of time, since both forward and reverse potential sweeps are symmetrical in relation to the switching potential (E_{λ}). On the other end, **Figure 6-B** presents the system current response to the applied potential, where the inversion point observed, when the positive current is converted in negative current, coincides with the switching potential.[70, 71]

Figure 6-C shows a typical cyclic voltammogram obtained for the reversible system ferrocyanide/ferricyanide ($[Fe(CN)_6]^{4-}/[Fe(CN)_6]^{3-}$) at a gold screen printed electrode (AuSPE) surface. According to the IUPAC convention, the negative current is referred to as the cathodic scan and the positive current as the anodic scan, corresponding to the reduction and oxidation processes that occur in the electrochemical system, respectively.[67, 68] For the $[Fe(CN)_6]^{4-}/[Fe(CN)_6]^{3-}$ redox system, the oxidation of ferrocyanide to ferricyanide corresponds to the anodic current peak ($I_{p,a}$). When the potential scan is reversed, after the inversion point, the reduction of ferricyanide back to ferrocyanide at the electrode surface is promoted and characterized by the cathodic current peak ($I_{p,c}$).

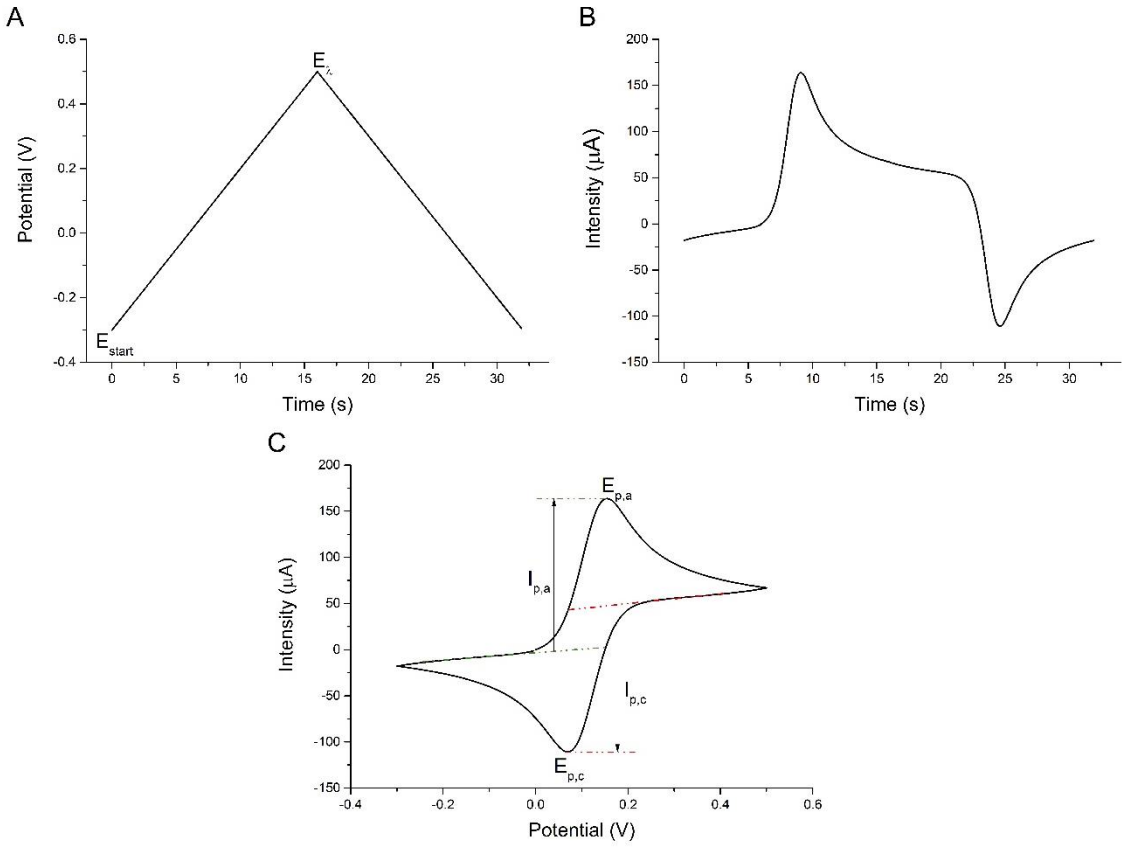

Figure 6 – Representation of the typical CV plots: **A –** potential *vs* time; **B –** current intensity *vs* time; **C –** current intensity *vs* potential (known as CV voltammogram) obtained for the reversible system ferrocyanide/ferricyanide at a gold screen-printed electrode surface. The data presented was collected during experimental procedures. The peak separation observed was of 85 mV, probably due to the use of a AuSPE and its ink composition.[72] A ratio between the peak current intensities of approximately 1 was observed.

To perform analytical studies, sometimes CV is used through the Randles-Sevcik equation (at 25 °C):

$$I_p = 2.686 \times 10^5 . n^{\frac{3}{2}} . A . C_0 . D^{\frac{1}{2}} . v^{\frac{1}{2}} \quad \textbf{(1)}$$

where I_p is the current intensity of the peak; n is the number of electrons involved in the reaction; A is the electrode area (cm^2); D is the diffusion coefficient ($cm^2\ s^{-1}$); C_0 is the species concentration ($mol\ cm^{-3}$) and; v is the scan rate ($V\ s^{-1}$). It is important to notice that this equation is only valid for reversible redox systems controlled by diffusion.[69, 73] If the process follows these conditions, the voltammogram must present the following characteristics:[74]

- The peak potentials maintain constant with variations of the scan rate;
- The peak current intensity is proportional to the square-root of the scan rate. If not, the process might be controlled by adsorption;

- The ratio between the current intensity of the anodic and cathodic peaks is equal to 1;
- The formal reduction potential (E^0) can be calculated using the anodic and cathodic peak potentials;

$$E^0 = \frac{E_{p,a}+E_{p,c}}{2} \quad \textbf{(2)}$$

- The separation in the anodic and cathodic peak potentials is close to 59 / n mV (at 25 °C).

2.4.2. Square-wave voltammetry

SWV is a pulse voltammetry technique where a potential pulse is applied on an electrode in function of time, that varies with a defined amplitude (ΔE) in a staircase waveform, with a step potential also defined (E_{step}) (see **Figure 7-A**).[75, 76] The current intensity is measured at the end of the forward pulse (I_1) and at the end of the reverse pulse (I_2). The signal is determined as the difference between I_1 and I_2, giving the intensity peak current (I_{peak}) observed in the SWV voltammogram (see **Figure 7-B**).[71, 75] In this voltammogram, the anodic current peak is observed and corresponds to the oxidation of ferrocyanide to ferricyanide.[67]

In accordance to Aoki *et al.*[76], the peak current intensity for plane electrodes can be calculated using the following equation:

$$I_{peak} = 0.9653.n.F.A.c.\left(\frac{D}{\tau}\right)^{\frac{1}{2}}.\tanh\left(\frac{\zeta}{2}\right) \quad \textbf{(3)}$$

where I_{peak} is the SWV peak current intensity; n is the number of electrons involved in the reaction; F is the Faraday constant (F = 96485 C mol^{-1}); A is the electrode area (cm^2); C_0 is the species concentration (mol cm^{-3}); D is the diffusion coefficient (cm^2 s^{-1}); τ is the square wave period (s) and; ζ is the dimensionless electrode potential. Thus, to improve the sensitivity of SWV and peak resolution obtained, the experimental parameters that can be controlled are: the pulse amplitude (ΔE_p) and the square-wave frequency (f), which corresponds to the inverse of the period. In less extent, the step potential (ΔE_s) and the stabilization time can also be optimized.[74]

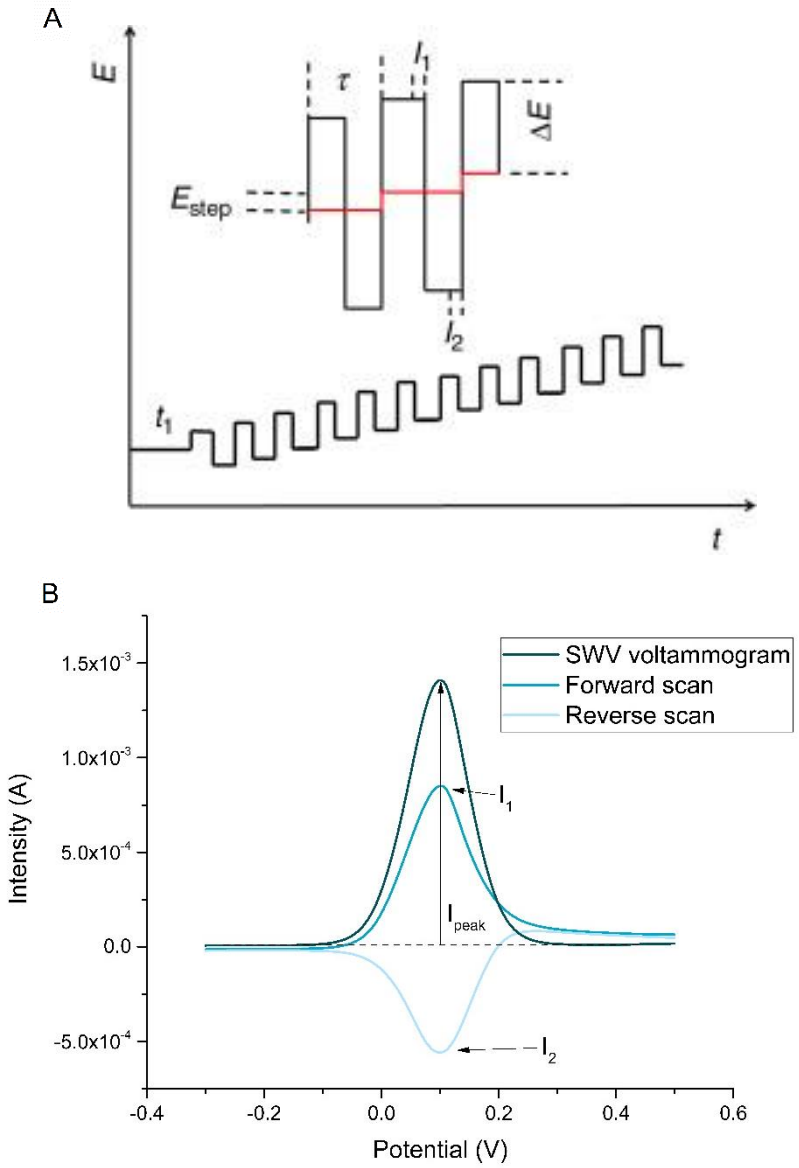

Figure 7 – Representation of the typical SWV plots: **A –** potential applied *vs* time (adapted from reference[71] with permission from Elsevier); **B –** current intensity *vs* potential (known as SWV voltammogram) obtained for the reversible system ferrocyanide/ferricyanide at a gold screen printed electrode surface. The data presented was collected during experimental procedures.

In electroanalytical studies, SWV shows better performance when compared to other electrochemical techniques (such as CV, DPV, etc.), due to its fast time of analysis, of only a few seconds, and higher sensitivity.[67, 71] A variety of works used SWV for fast and sensitive detection of cardiac biomarkers[77, 78].

3. Materials and methods

In this section, all the reagents, materials, experimental apparatus (electrochemical, AFM and SEM) and procedures used in this work are presented and described.

3.1. Reagents

All the reagents used to accomplish the work are listed in **Table 1**.

Table 1 – Reagents used in this work.

Name	Formula/Acronym	Purity (%)	Company
Sulfuric acid	H_2SO_4	95 - 97	Merck
Potassium ferricyanide	$K_3[Fe(CN)_6]$	≥ 99	Fluka
Potassium ferrocyanide trihydrate	$K_4[Fe(CN)_6]\cdot 3H_2O$	≥ 99.5	Fluka
Sodium sulphate	Na_2SO_4	p.a.	Merck
Sodium dihydrogen phosphate monohydrate	$NaH_2PO_4\cdot H_2O$	p.a.	Merck
Sodium phosphate dibasic dihydrate	$Na_2HPO_4\cdot 2H_2O$	p.a.	Sigma-Aldrich
Dopamine	DA	98	Sigma-Aldrich
Atrial natriuretic peptide	ANP	93.35	United peptide
Sodium acetate trihydrate	$CH_3COON_a\cdot 3H_2O$	p.a.	Merck
Acetic acid	CH_3COOH	96	Merck
Sodium dodecyl sulphate	SDS	≥ 98.5	Sigma-Aldrich
Sodium hydroxide	NaOH	≥ 97	Sigma-Aldrich
Oxalic acid		≥ 99	Sigma-Aldrich
ANP epitope	NH_2-CNSFRY-COOH (aminoacid sequence)	≥ 95	GenScript

All the aqueous solutions were prepared using ultrapure water purified with a Milli-Q purification system (resistivity ≥ 18MΩ cm). Stock solution of phosphate buffer (PB) 1.0 mol L^{-1}, pH 6.9, was prepared using $NaH_2PO_4 \cdot H_2O$ and $Na_2HPO_4 \cdot 2H_2O$ salts. Fresh working buffer solution (C = 0.1 mol L^{-1}; pH 7.2) was prepared by dilution of previous concentrated PB solution.

For the detection studies, fresh ANP standard solutions were daily prepared before the experiments. Firstly, a 1.0 mmol L^{-1} ANP solution was prepared in PB 0.1 mol L^{-1}, pH 7.2 and then less concentrated ANP standard solutions (concentrations ranging from 1.0 µmol L^{-1} to 500.0 µmol L^{-1}) were prepared by suitable dilution in PB solution.

3.2. Electrochemical analysis

In this subchapter, the electrochemical setup used in this work and the subsequent experimental conditions from biosensor construction to analysis are described.

3.2.1. Electrochemical setup

Electrochemical data was obtained using a computer-controlled potentiostat PalmSens controlled by the software PSTrace 5.9 (**Figure 8-A**).

Gold screen-printed electrodes (AuSPEs) were purchased from Metrohm (DropSens DRP-220AT) (**Figure 8-B**). The three electrodes, the working electrode consisting of a gold disk, the pseudo-reference electrode based on a silver ink, and the gold counter electrode, were all screen-printed on a ceramic substrate and subjected to high-temperature curing. The electric contacts are made of silver ink.

A switch box from DropSens (DRP-DSC) was used to connect the AuSPEs to the potentiostat (**Figure 8-A**).

The collected electrochemical data was processed using the software OriginPro 2016.

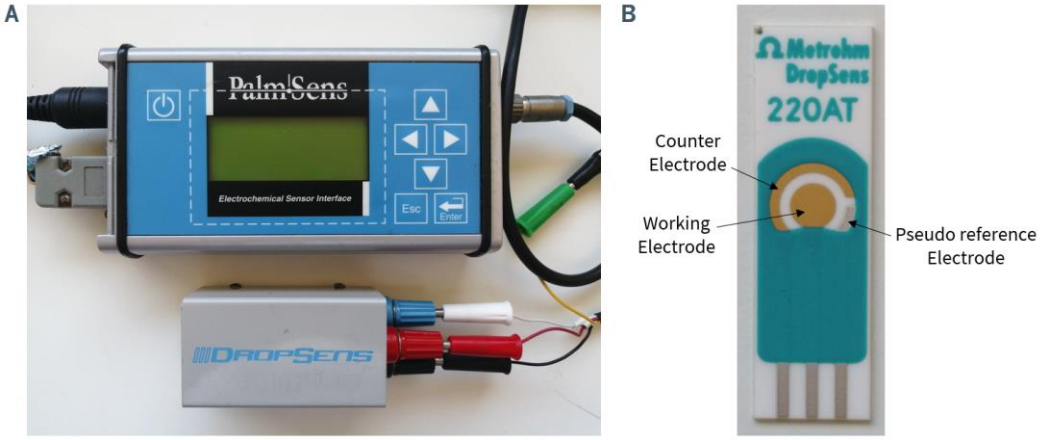

Figure 8 – Set up for electrochemical analysis. **A –** PalmSens potentiostat connected to the DropSens switchbox. **B –** AuSPE used for electrochemical detection of ANP.

3.2.2. Electrochemical measurements

For the electrochemical measurements, a solution of 5 mmol L^{-1} $[Fe(CN)_6]^{4-}/[Fe(CN)_6]^{3-}$ was prepared in a 0.1 mol L^{-1} sodium sulphate as electrolyte and used as redox probe (60 µL drop). This mixture solution, identified as hexacyanoferrate (HCF), was used to monitor the polymer formation on the electrode and for ANP electroanalysis by considering the peak current intensity (I_p) decrease due to the inhibition of redox probe permeation to the electrode surface.

Both CV and SWV were recorded in the potential range of -0.30 V to 0.50 V. CV was performed using a scan rate of 50 mV s^{-1} and SWV was operated with a step potential of 2 mV, a pulse amplitude of 50 mV and a frequency of 25 Hz.

All experiments were conducted at room temperature (RT).

3.2.3. Biosensor construction

Before modification, the AuSPEs were washed with water and ethanol, and dried under a nitrogen flow. Then, the electrochemical cleaning of the electrode surface was performed using the CV technique in 0.5 mol L^{-1} H_2SO_4 solution (60 µL drop). A potential scan from 0 to 1.15 V was applied, at a scan rate of 0.1 V s^{-1}, during approximately 10 cycles (until the voltammogram was stable). Finally, the AuSPEs were washed with pure water and dried under nitrogen flow. The washing procedure was repeated after surface

modification, incubation with standard solutions and electrochemical measurement in the presence of the redox probe solution.

For the MIP film formation by electropolymerization, dopamine (DA) was used as electroactive monomer and ANP was used as the template molecule. After optimization of the experimental conditions (template extraction procedure, film thickness and template concentration), the procedure for the biosensor construction is schematic represented in **Figure 9** and englobes:

1 – Electropolymerization of dopamine (DA), using the CV technique, after covering the electrode surface with a 60 µL drop of a 2 mmol L^{-1} DA solution containing 0.5 mg mL^{-1} of ANP in PB 0.1 mol L^{-1}, pH 7.2. The DA solution was freshly prepared before use. For CV polymerization, the potential was cycled from -0.7 to 0.7 V, at a scan rate of 0.05 V s^{-1}, during 6 cycles.

2 – Extraction of template molecule. The washing procedure was performed by immersing the chips in acetate buffer 0.05 mol L^{-1}, pH 4.5, containing 5 % (w/v) SDS, overnight under gentle agitation.

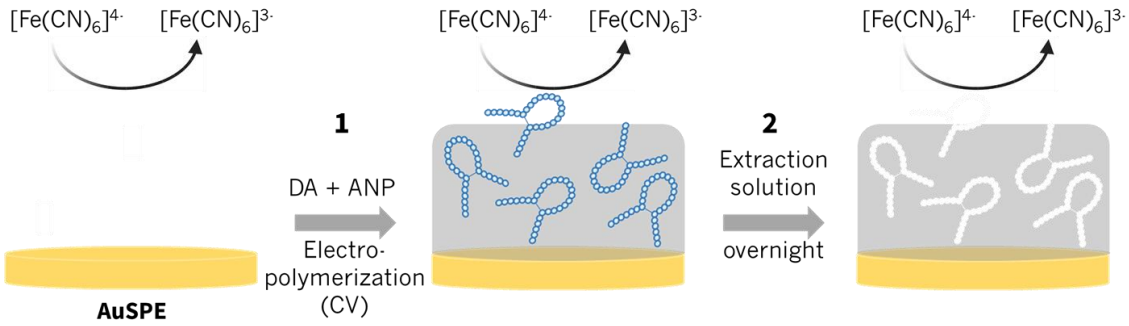

Figure 9 – Schematic representation of the biosensor construction. After each modification step, the AuSPE surface was characterized by CV and SWV techniques using the couple $[Fe(CN)_6]^{4-}/[Fe(CN)_6]^{3-}$ as a reporting system.

In parallel, a non-imprinted polymer (NIP) was also prepared in the same way as the MIP but in the absence of the template peptide. The NIP works as a reference system that characterizes the non-specific adsorption that occurs on the surface of the sensor due to the absence of specific binding sites to recognize the target analyte.

3.2.4. Detection studies

Firstly, the electrode surface was incubated with 60 µL of PB 0.1 mol L^{-1}, pH 7.2, for 2 minutes, washed with pure water and dried under nitrogen flow, and electrochemically characterized with the redox probe. This procedure was repeated until stable peak intensity was obtained (surface stabilization). In the end, to replicate the same conditions as applied to the samples, the electrode was incubated with PB for 15 minutes and SWV measurements were performed to collect the baseline.

After acquiring the baseline, the biosensor surface was incubated for 15 minutes with ANP standard solutions (concentrations ranging from 1.0 µmol L^{-1} to 1.0 mmol L^{-1}, prepared in PB 0.1 mol L^{-1}, pH 7.2), washed with pure water and dried under nitrogen flow. Then, SWV measurements in the presence of the redox probe were performed on the biosensor surface.

This process was done for both the MIP and NIP and repeated over several days to evaluate the day-to-day reproducibility of the biosensor preparation and response to the target analyte.

The calibration curve was obtained by representing the SWV peak intensity as a function of ANP concentration logarithm (I (mA) *vs* log [ANP (µmol L^{-1})]). From the obtained calibration curve, the sensitivity of the biosensor and the respective limit of detection (LOD) achieved were estimated. The LOD was determined according to the IUPAC recommendation for ion-selective electrodes.[79]

3.2.5. Selectivity studies

A study of the biosensor response to other molecules was performed to evaluate the biosensor selectivity. The biomolecules selected for this study were: (i) bovine serum albumin (BSA); (ii) vancomycin and; (iii) myoglobin. The biosensor response for each interferent was recorded at a concentration of 500 µmol L^{-1} prepared in PB 0.1 mol L^{-1}, pH 7.2, and compared with the response obtained for the target analyte.

3.2.6. Biosensor construction using epitope imprinting approach

Knowing the advantages of using the epitope imprinting approach, the biosensor was also constructed using an epitope from ANP as template. The epitope chosen as a unique aminoacid sequence from ANP was the C-terminal, presented in **Figure 10**.

Figure 10 – ANP epitope used in this work as template for imprinting. Aminoacid one letter code: C – cysteine; N – asparagine; S – serine; F – phenylalanine; R – arginine; Y – tyrosine.

The biosensor was constructed following the same procedure presented previously on **3.2.3.**, except, the ANP epitope is present in the polymeric solution instead of the ANP molecule, but in the same concentration, 0.5 mg mL^{-1}. This biosensor will further be referred as epitope molecularly imprinted polymer (EMIP). A detection study was performed in the same conditions as described on **3.2.4.**.

3.2.7. Biosensor application for ANP-nanoparticles detection

As stated before, the biosensor was developed for the detection of ANP functionalized nanoparticles (NPs), used as a drug delivery system for the treatment of cardiovascular diseases. This part of the work was performed in the Santos' Lab group (Netherlands). The poly(lactic-co-glycolic acid) (PLGA) nanoparticles were synthesized using a microfluidic system followed by covalent attachment of ANP through 1-ethyl-3-(3-dimethylaminopropyl)carbodiimide (EDC)/ N-hydroxysuccinimide (NHS) coupling. From now on, they will be referred to as PLGA-NPs@ANP. Non-functionalized nanoparticles, identified as PLGA-NPs, were also used in this work to evaluate the specificity given to the particles by the functionalization with ANP and the specificity of the MIP to the functionalized NPs, acting similarly to a NIP system.

To assess the biosensor response, detection studies were performed as described on **3.2.4.** but using NPs standard solutions with increasing concentration ranging from 4.0 µg mL^{-1} to 100.0 µg mL^{-1} in PB 0.1 µmol L^{-1}, pH 7.2.

The calibration curve was obtained by representing the SWV peak intensity as a function of NPs concentration logarithm, I (mA) *vs* log (NPs (µg mL^{-1})).

3.3. AFM analysis

To assess the morphology of the film, atomic force microscopy (AFM) measurements were performed on the working electrode of the AuSPE before and after electropolymerization of DA at the electrode surface. A scan size of 150 µm was used to obtain the AFM images. No prior sample preparation was required, and all experiments were conducted at RT.

AFM analysis was accomplished using a BioScope Catalyst (Bruker) with a silicon tip on nitride lever (Bruker, SCANASYST-AIR model) with a resonance frequency of 70 kHz (see **Figure 11**). The collected data was processed using the software NanoScope Analysis 2.0 and Gwyddion.

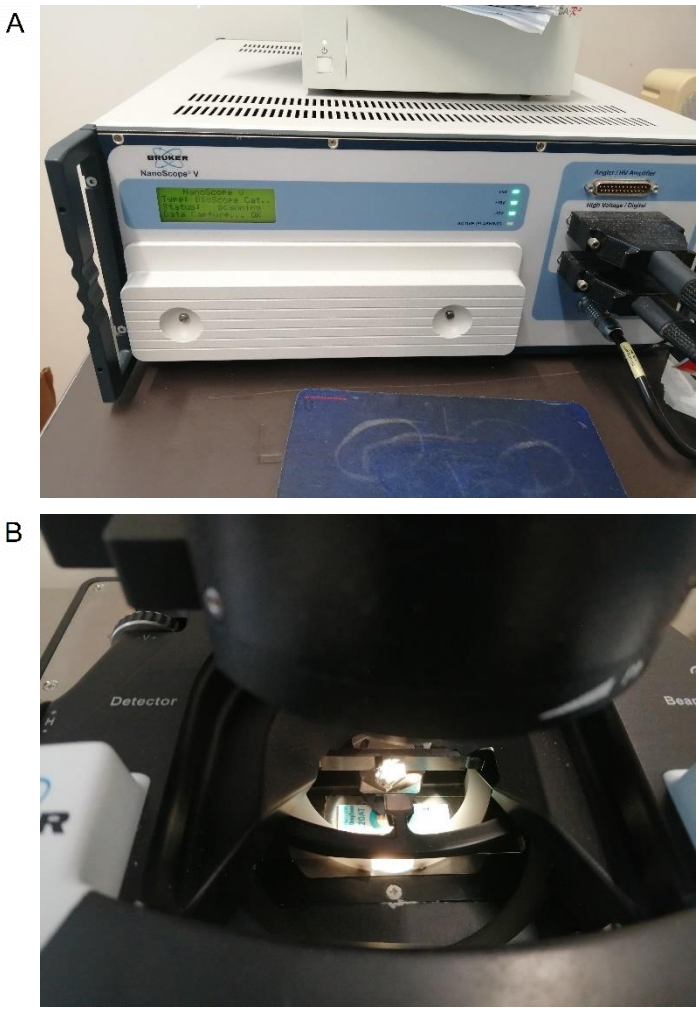

Figure 11 – AFM analysis setup. **A –** Bruker AFM equipment. **B –** Representation of a probe measuring at the SPE surface.

3.4. SEM analysis

Scanning electron microscopy (SEM) images of the MIP surface before (bare) and after electropolymerization, and after template extraction, were obtained with magnification of 11.26K X. SEM analysis was accomplished using a Supra 55 (Zeiss) (see **Figure 12**) controlled by the image acquisition software Atlas 5.2.

Prior to analysis, the AuSPE was attached to a sample support (an aluminium mount - Slotted Head, 6 mm H, Electron Microscopy Sciences - with a carbon adhesive tape on top - Dia Electron Microscopy Sciences, Size 12 mm), followed by a subsequent sample chromium coating using a Leica EM ACE600 Sputter Coater (Leica Microsystems). The sputtering was performed under the following conditions: current of 110 mA, pressure of 1.0×10^{-2} mbar, working distance of 50 mm, no tilt, and a film thickness of 5.0 nm.

All experiments were conducted at RT.

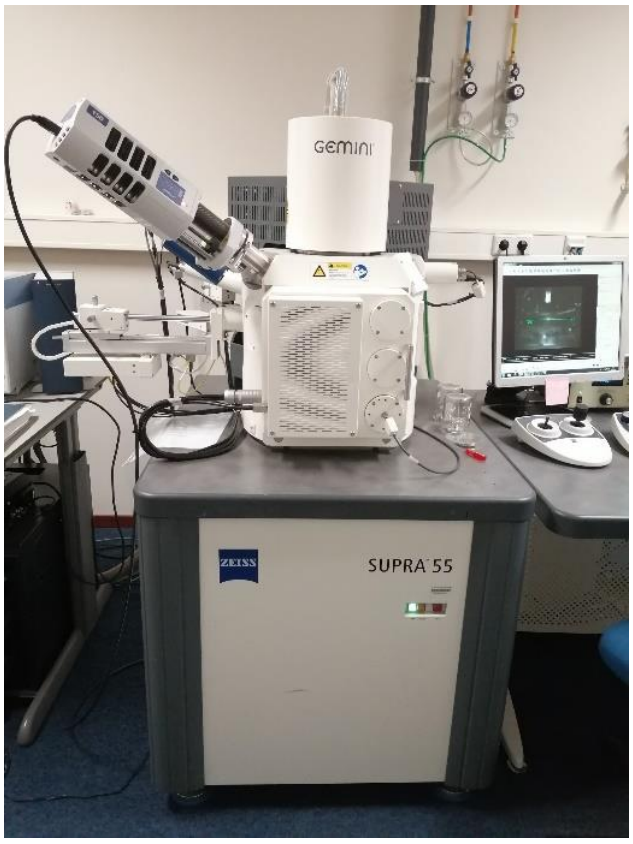

Figure 12 – SEM equipment used in this work.

4. Results and discussion

In this section, the results obtained along this work, from the MIP film production, optimization of the experimental conditions until the biosensor construction and respective application, are reported and discussed.

4.1. MIP production by dopamine electropolymerization

Dopamine (DA) was used as the redox-active monomer for MIP film production due to its high biocompatibility and hydrophilic nature.[55] As stated in the literature overview, the polydopamine formation can occur under alkaline conditions or by the use of electrochemical techniques.[50]

Given the possibility of DA self-polymerization, preliminary studies were performed to evaluate the stability of the DA solution in PB 0.1 mol L^{-1}, pH 7.2, along the time using ultraviolet-visible (UV-Vis). The results obtained, shown in **Annex 1**, do not show relevant differences in maximum absorbance over time allowing to affirm that the DA solution maintains its properties (without self-polymerization) during the working time. Thus, in this work, for MIP receptor film deposition on the electrode surface, CV technique was chosen to polymerize DA.

Figure 13-A shows the representative CV curves recorded during the electropolymerization of a 2 mmol L^{-1} DA solution in PB 0.1 mol L^{-1}, pH 7.2, on an AuSPE at a scan rate of 50 mV s^{-1} (NIP film; 6 CV cycles). As can be seen, four peaks can be observed: an anodic peak at 0.10 V, identified as Pa_1; two cathodic peaks at 0.04 V and -0.35 V, identified as Pc_1 and Pc_2, respectively; and another anodic peak at -0.29 V, identified as Pa_2. According to the proposed mechanism presented by Wang *et al*.[80] (**Figure 13-B**), the observed voltammetric responses are associated to the following redox couples: dopamine/dopaminequinone (Pa_1/Pc_1) and leucodopaminechrome/dopaminechrome (Pa_2/Pc_2). A decrease in all the peak currents, as well as an increase in peak-to-peak separations between the redox couples previously identified, is observed as the number of potential scans applied increases. This electrochemical behaviour was due to the formation and growth of a non-conductive polydopamine film at the electrode surface, which inhibits the permeation of DA through the film for further oxidation.[80, 81]

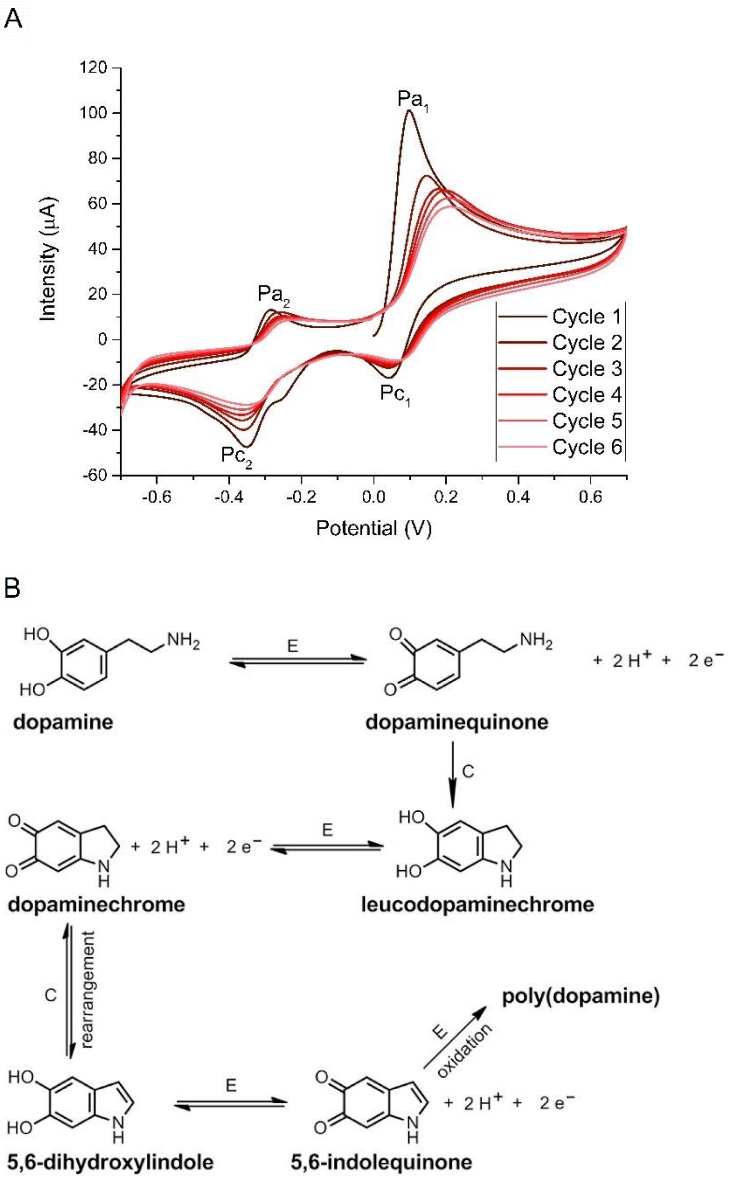

Figure 13 – A – Electropolymerization of dopamine solution (2 mmol L^{-1} in PB 0.1 mol L^{-1}, pH 7.2) by CV - 6 cycles. The scan rate was 50 mV s^{-1}. **B –** Proposed mechanism for the electropolymerization of DA. "E" - Electrochemical reactions; "C" - chemical reactions. Adapted from reference[80] with permission from Elsevier.

The MIP films were prepared in the same way. The representative CV curves recorded during the electropolymerization of DA in the presence of the template are present in **Annex 2**. Although the CV electrochemical behaviour due to DA polymerization was quite similar, an overall decrease of the peak current intensity was observed. In this case, not only the MIP film growth prevents further DA oxidation, but also the template adsorption on the electrode surface and physical entrapment within the polydopamine film promotes an additional blockage to DA diffusion, decreasing the current intensity recorded.

4.2. Optimization of experimental conditions

To develop the MIP-based biosensor for ANP detection, the experimental conditions were first optimized, namely: the template extraction procedure, the template concentration used and the polydopamine film thickness. The different steps of the MIP construction were monitored by performing electrochemical measurements in the presence of 5 mmol L^{-1} HCF.

As stated before, an efficient template extraction is a crucial part of the imprinting process that will later affect the biosensor selectivity and sensitivity.[60] For ANP extraction from the polydopamine film, three solutions were tested: (i) acetate buffer 0.05 mol L^{-1}, pH 4.5, containing 5 % (w/v) SDS, (ii) oxalic acid 5 mmol L^{-1} and (iii) NaOH 1 mol L^{-1}. All extraction procedures were done overnight, under gentle agitation. In parallel, possible damage induced by the extraction solution on the polymeric matrix was evaluated at the NIP system.

As can be seen in **Figure 14**, the solutions of oxalic acid and sodium hydroxide promoted a huge increase in the SWV current intensity at the NIP surface, meaning that the polydopamine film was damaged after being in contact with these extraction solutions. In the case of the acetate buffer solution containing SDS, a minimum intensity increase on the NIP was observed, indicating that the polydopamine film remained intact. For the MIP surface, the results showed considerable increase in the HCF peak current intensity due to the successful template removal from the polymeric matrix, which promotes the diffusion of the probe species through the film empty cavities to the electrode surface.

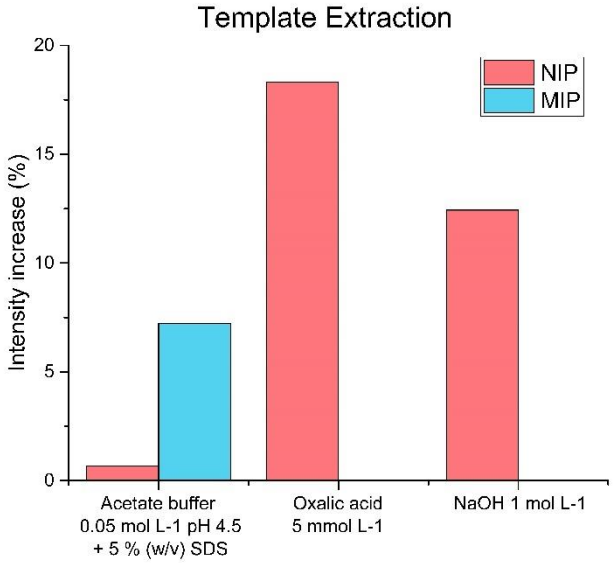

Figure 14 - Optimization of the template extraction procedure for MIP construction (template concentration - 0.5 mg mL^{-1}) by monitoring the HCF SWV current intensity increase, expressed in terms of signal percentage (%), after treating the MIP and NIP surfaces with the tested extraction solutions, overnight.

The polymer film thickness is also an important characteristic of a MIP that affects the overall performance of the biosensor.[82] If the film is too thick, the extraction procedures are made difficult, as the template molecules are not accessible in the polymeric matrix. On the other hand, a film too thin leads to malformed binding sites and bad recognition of the target analyte, therefore to low selectivity. Also, the electrode surface can be exposed promoting the non-specific adsorption. Thus, the optimal film thickness should be similar to the biomolecule size.[82]

In this work, the film thickness was optimized taking into consideration two fundamental conditions. First, the electropolymerization conditions were optimized to block the gold surface with the polydopamine hydrophilic polymer aiming to minimize the non-specific adsorption.[83] Thus, the permeation of the redox probe through the film was evaluated after DA electropolymerization applying different number of CV cycles (1, 2, 5, 10 and 20) to determine the best insulating conditions (see **Figure 15-A**). The results obtained show that full surface blockage is achieved by performing 5 or more CV cycles during the electrochemical polymerization.

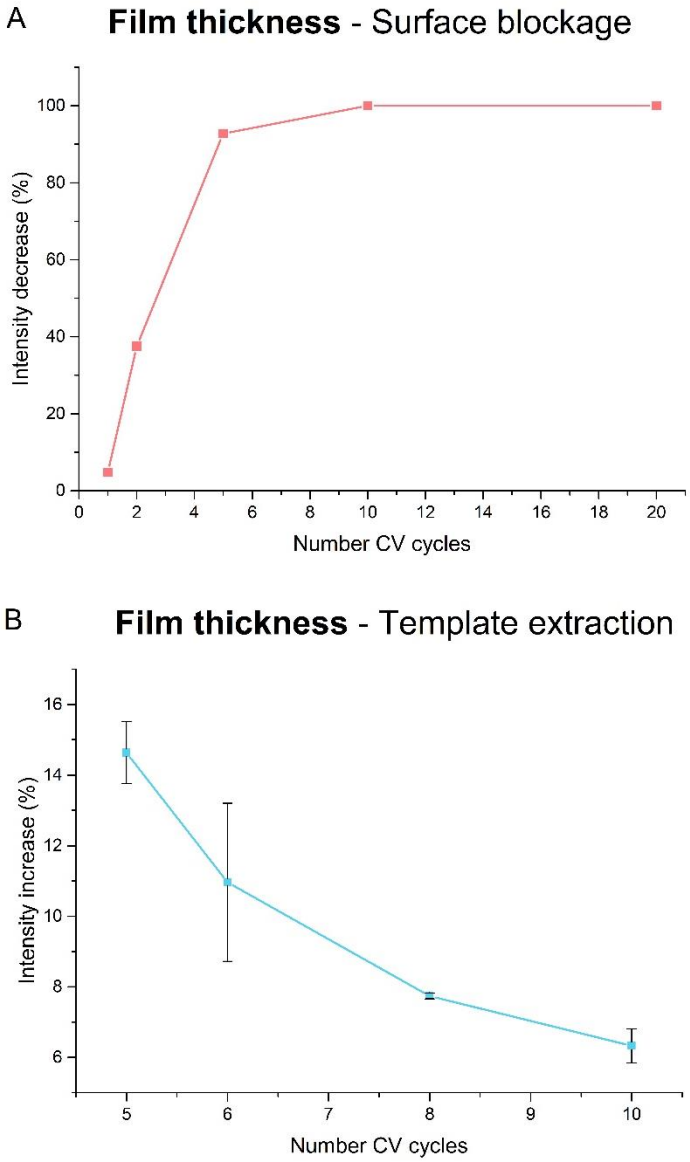

Figure 15 - Optimization of MIP film thickness. **A –** HCF peak **c**urrent **i**ntensity decrease, expressed in terms of signal percentage (%), after electropolymerization of DA for the NIP construction. **B –** HCF peak current intensity increase, expressed in terms of signal percentage (%), after the extraction of the template from the MIP polymeric matrix (template concentration - 0.5 mg mL^{-1}). Duplicate assays were performed (n = 2).

In the second part of the film thickness optimization, a balance between effective template extraction and high surface blockage was envisage. To determine the optimal number of CV cycles for the MIP film construction, the template extraction efficiency in relation to the number of CV cycles applied (5, 6, 8 and 10) to the polymeric solution was evaluated, as show in **Figure 15-B**. The template concentration used in this study was of 0.5 mg mL^{-1}. After analysing the data shown in the figure, 6 CV cycles were chosen as optimal for MIP preparation by electropolymerization.

Lastly, the effect of template concentration in the polymerization solution was investigated. A sufficient number of template molecules needs to be present in the solution to increase the number of imprinting cavities in the polymeric matrix for improved sensor response (high linear response range). On the other end, excessive number of template molecules in solution might promote intermolecular interactions between the molecules (aggregation) creating overlapped cavities or cavities with poor shape-complementary that can reduce the selectivity of the MIP film to the target analyte. In addition, ANP peptide obtained commercially is very expensive which makes lowering the template concentration desirable to minimize the biosensor production cost without compromising the MIP ability to recognize the target analyte.

To study this effect, ANP concentrations on the polymerization solution ranging from 0.001 to 1.0 mg mL^{-1} were tested, maintaining constant the 6 CV cycles for the electropolymerization and then treating the MIP surface with the extraction solution (acetate buffer 0.05 mol L^{-1}, pH 4.5, containing 5 % (w/v) SDS). From the results obtained, shown in **Figure 16**, the ANP concentration chosen for MIP production was 0.5 mg mL^{-1}.

The possibility of using 0.1 mg mL^{-1} of ANP was also studied in this work (results not shown), but the results obtained revealed that such concentration level of template conferred lower sensitivity to the MIP sensor when compared to 0.5 mg mL^{-1}.

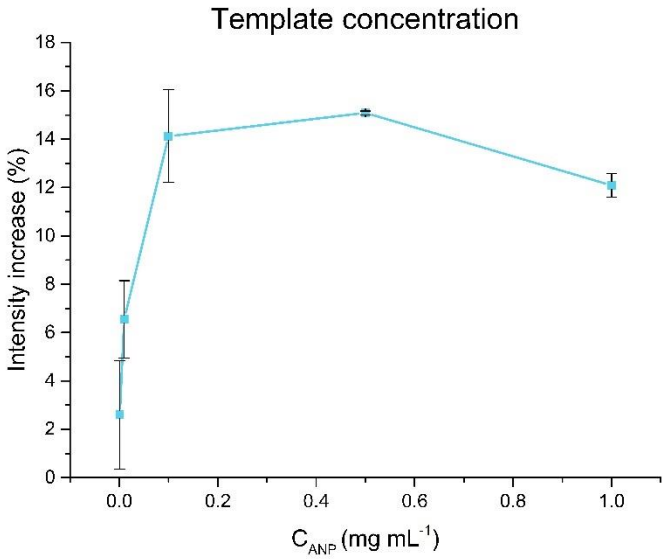

Figure 16 – Optimization of the template concentration (using 6 CV cycles). HCF peak current intensity increase, expressed in terms of signal percentage (%), after the extraction of the template (0.001, 0.01, 0.1, 0.5 and 1.0 mg mL^{-1}) from the MIP polymeric matrix. Duplicate assays were performed (n = 2).

To sum up, the optimized experimental conditions used in this work for the construction of the MIP receptor film were:

- monomer – DA 2 mmol L^{-1};
- template concentration - ANP 0.5 mg mL^{-1};
- film thickness - 6 CV cycles at a scan rate of 0.05 V s^{-1};
- template extraction procedure - acetate buffer 0.05 mol L^{-1}, pH 4.5, containing 5 % (w/v) SDS, overnight under gentle agitation.

4.3. Biosensor characterization

4.3.1. Electrochemical characterization

The step-by-step modification of the sensor surface was confirmed by electrochemical measurements, using CV and SWV techniques, and includes voltammetric measurements before (bare gold surface) and after electropolymerization, and after template extraction from the polymeric matrix. To obtain reliable results, MIP and NIP constructions were performed in parallel. Representative voltammograms recorded are shown in **Figure 17** for both systems.

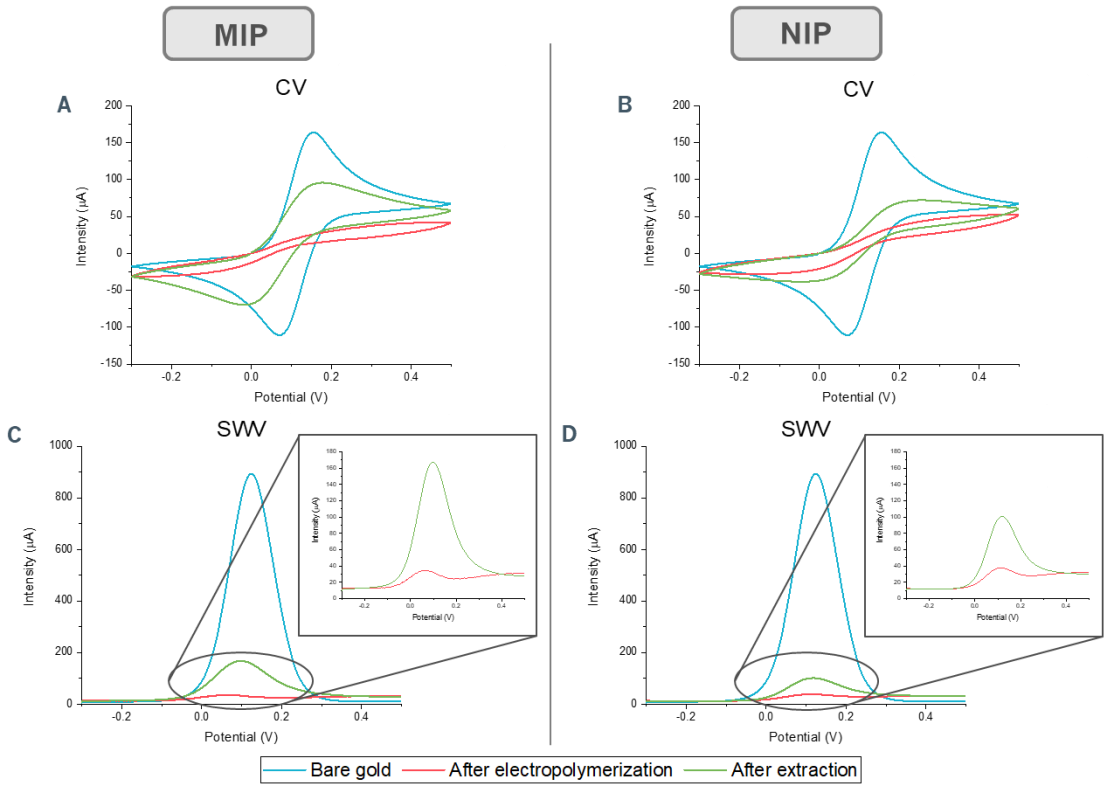

Figure 17 – Representative voltammograms, obtained in the presence of 5 mmol L^{-1} HCF, of the step-by-step modification of the electrode surface for construction of the **(A,C)** MIP receptor film (monomer concentration of **2 mmol L^{-1} DA**; **6 cycles** of CV for the electropolymerization; template concentration of **0.5 mg mL^{-1} ANP**; extraction with **acetate buffer 0.05 mol L^{-1} pH 4.5 + 5 % (w/v) SDS, overnight**) and the **(B,D)** NIP receptor film. **A, B –** CV measurements and; **C, D –** SWV measurements recorded before (bare gold) and after DA electropolymerization, and after template extraction.

Focusing on **Figure 17-A** and **C**, the CV and SWV characterization of the MIP surface, respectively, revealed the successful electropolymerization of the monomer solution leading to the effective MIP film formation on the gold surface, which inhibited the redox probe diffusional permeation through the film to the electrode surface. After the template extraction from the polymeric matrix, an increase of peak current intensity was observed due to the more favoured permeation of the redox probe through the empty molecular cavities formed on the polymer to the electrode surface, as predicted by the gate effect that occurs in MIPs films for protein recognition.[63]

Comparing with the results obtained for the reference system, represented on **Figure 17-B** and **D**, a small peak current intensity increase was observed after exposure of the NIP surface to the extraction solution. This was probably due to the removal of loosely bound monomer molecules adsorbed to the gold electrode surface or incorporated within the polymeric matrix.

4.3.2. AFM characterization

AFM technique can be very useful to characterize and obtain morphological information on MIP structures on electrode surfaces.[84] In this work, AFM characterization was performed on the working electrode of the SPE before (bare gold) and after electropolymerization of dopamine. The collected AFM images are shown in **Figure 18**.

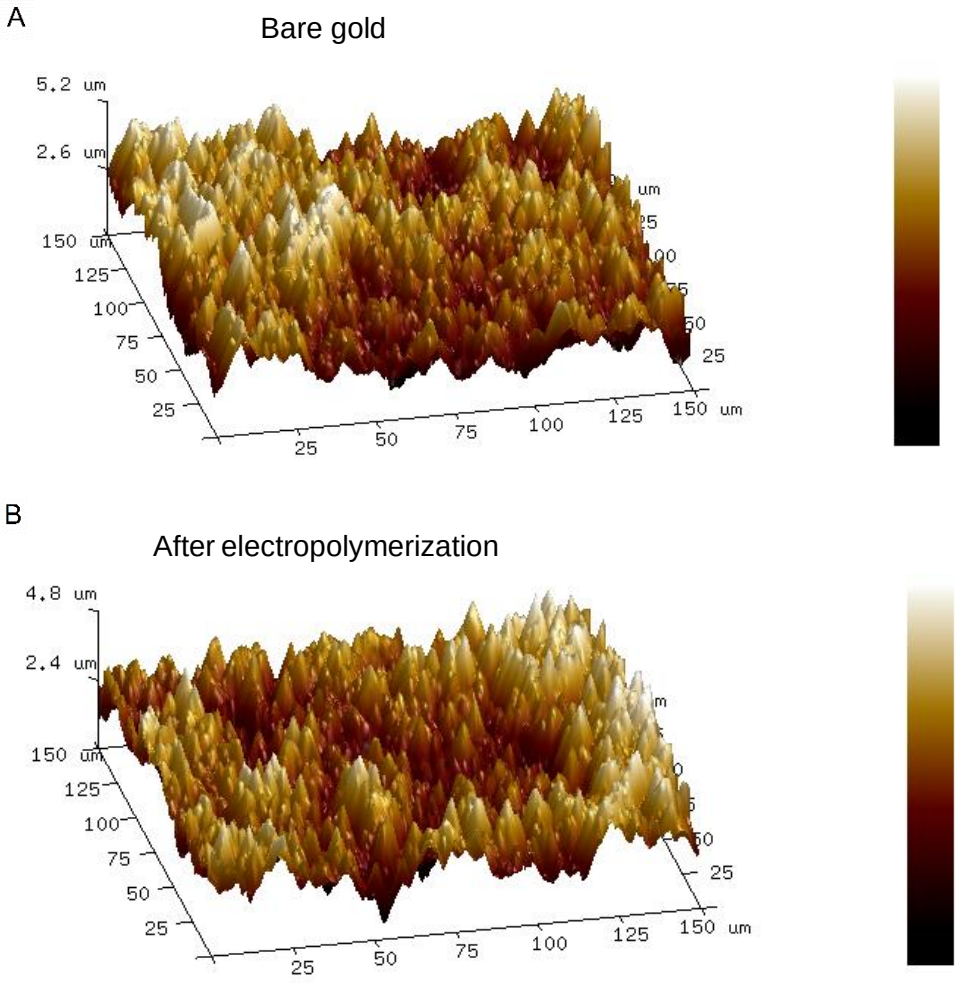

Figure 18 – AFM 3D-images of the gold SPE surface. **A –** Bare gold surface; **B –** After polymer deposition on the electrode surface by electropolymerization.

As can be seen, the bare gold surface presents a high rough profile which is characteristic of SPEs. This is associated to the fabrication process of the screen-printed chips in which an ink containing gold (nano/micro)particles in suspension is randomly deposited in the surface and is later cured.[85] The root mean square (RMS) surface roughness obtained, of 632.2 nm, was in accordance with this observation. After DA electropolymerization, the RMS value decreased to 578.4 nm, meaning that the surface

becomes smoother after polydopamine film formation over the gold surface, filling the existent cavities (valleys) in the bare gold with the film. Furthermore, the surface depth of the modified electrode (4.8 µm) decreased relatively to the bare gold surface (5.2 µm).

The results obtained in this work are in accordance with the literature. In the work of Rebelo *et al.*[86], where a MIP-based electrochemical biosensor was developed for the detection of a stress biomarker amylase in human saliva, the AFM results showed a decrease of almost 40 nm in the RMS surface roughness after electropolymerization of pyrrole monomer on the AuSPE surface, accompanied with a decrease of approximately 1 µm of the surface depth of the film relatively to the bare surface, meaning that a smoother surface was obtained after the MIP film formation.

4.3.3. SEM characterization

SEM characterization of the electrode surface was also performed after each step of the biosensor construction to obtain a visual representation of the AFM images. The SEM images collected are shown in **Figure 19**.

As can be seen in **Figure 19-A**, the bare gold SPE is rough and heterogeneous with nanometre and micrometre-scale hills and valleys, as previously reported by Zamani *et al*.[87], and the absence of ink in some regions can be observed in the form of craters. After electropolymerization (**Figure 19-B**), the surface becomes smoother due to the coverage of the valleys with the polydopamine film and the disappearance of the craters can be observed due to the same reason. This is in accordance with the results obtained from AFM measurements, where the surface roughness decreases after electropolymerization.

After the extraction of the template molecule from the MIP film, the SEM image shows the presence of small cavities that were formed in the MIP film as a consequence of the template removal (**Figure 19-C**).

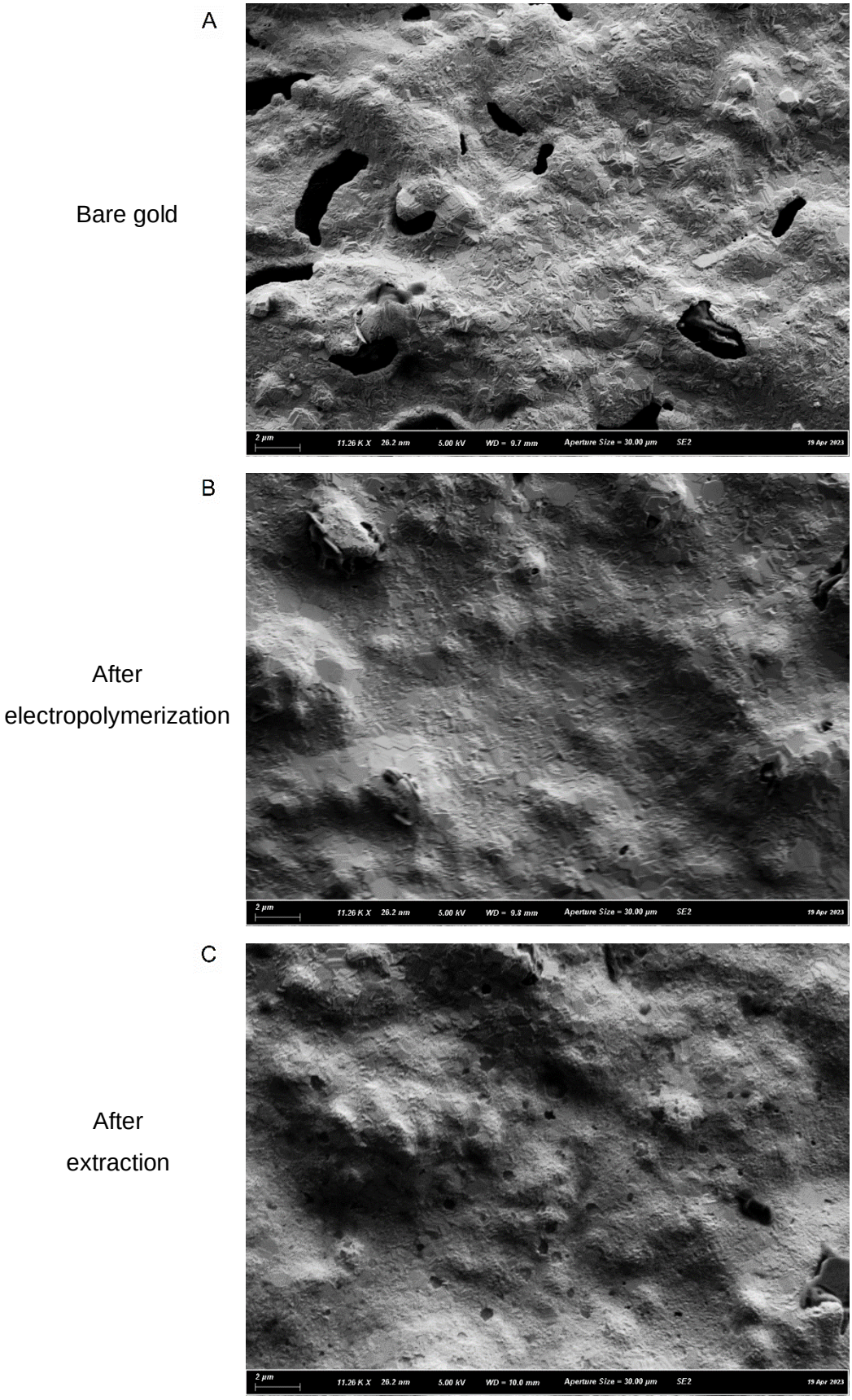

Figure 19 – SEM images of the gold SPE surface. **A –** Bare gold; **B –** surface after MIP formation by electropolymerization; **C –** surface after template extraction from the MIP film.

4.4. Analytical performance of the biosensor

In this sub-section, the results obtained to study the analytical performance of the developed MIP biosensor are presented, namely: calibration curves; fitting of adsorption models and estimation of affinity constants; selectivity of the biosensor against biomolecules chosen as interferents.

4.4.1. Detection studies

After optimization of the experimental conditions, the developed MIP biosensor was used for the detection and quantification of ANP in PB. After 15 minutes of incubation of the biosensor surface with target analyte solution (ANP standards ranging from 1.0 μmol L^{-1} to 1.0 mmol L^{-1}), SWV measurements in the presence of 5 mmol L^{-1} HCF were recorded, as shown in **Figure 20-A**.

During the rebinding events, the empty imprinted sites at the MIP film surface interact with target analyte, blocking the diffusional pathway of the redox probe to the electrode surface.[63] This event induces a decrease in the anodic peak of the redox probe with the increasing ANP concentration in solution that can be seen in **Figure 20-A**.

After estimation of the SWV peak current intensity, used as analytical signal, the corresponding calibration curve was built. A linear pattern against the concentration logarithm was observed (R^2 = 0.9963) for ANP concentration range from 1.0 μmol L^{-1} to 1.0 mmol L^{-1} (**Figure 20-B**, MIP) with a sensitivity of - 0.033 mA L μmol^{-1} $decade^{-1}$. The limit of detection (LOD < 1.0 μmol L^{-1}) was estimated according to the IUPAC recommendation for ion-selective electrodes.[79]

Some analytical features of other developed biosensors for ANP detection reported in the literature are presented in **Table 2**. Wang *et al.*[9] synthesized MIP NPs (nanoMIPs) by precipitation polymerization using the epitope imprinting approach and the detection was performed using a fluorescent assay. The LOD obtained (36.0 μmol L^{-1}) was higher than the one obtained in this work (LOD < 1.0 μmol L^{-1}).

When compared to the assays where natural antibodies were used as receptors, lower values of LOD were obtained. However, these immunoassays have the disadvantages of being complex, very expensive and present a high response time. Thus, the developed biosensor using MIP as receptor presents interest and potential for certain applications, with the possibility of being improved by using the epitope imprinting approach, for

example, in order to increase the number and accessibility of binding sites, increasing the sensitivity of the biosensor.

Table 2 - Comparison of the analytical features of the developed MIP biosensor with biosensors for ANP detection reported in the literature. ELISA – Enzyme-linked immunosorbent assay.

Receptor	Transduction mode	LOD (μmol L^{-1})	Reference
MIP NPs	Fluorescence	36.0	[9]
Antibody (sandwich immunoassay)	Chemiluminescence	1.3×10^{-7}	[7]
Antibody (ELISA kit)	Colorimetric	2.41×10^{-4}	[88]
MIP film	Electrochemical	< 1.0	This work

For comparison, the obtained NIP response to the ANP standard solutions was also included in **Figure 20-B**, where a non-linear response was observed, as expected, since only non-specific adsorption of target analyte can occur at this surface (absence of specific molecular cavities).

An imprinting factor (IF) of 2.1, calculated by the ratio of the SWV peak intensity for the concentration of ANP of 10 μmol L^{-1} between MIP and NIP, was obtained for the developed biosensor, indicating the existence of specific interactions between the target analyte and the imprinting cavities present in the synthetic receptor MIP film.

The obtained IF value was similar to others reported in the literature. For example, Erdem *et al.*[89] synthesized MIP particles in a micro-reactor for the detection of bovine serum albumin (BSA). In their work, an imprinting factor of 2.3 was reported.

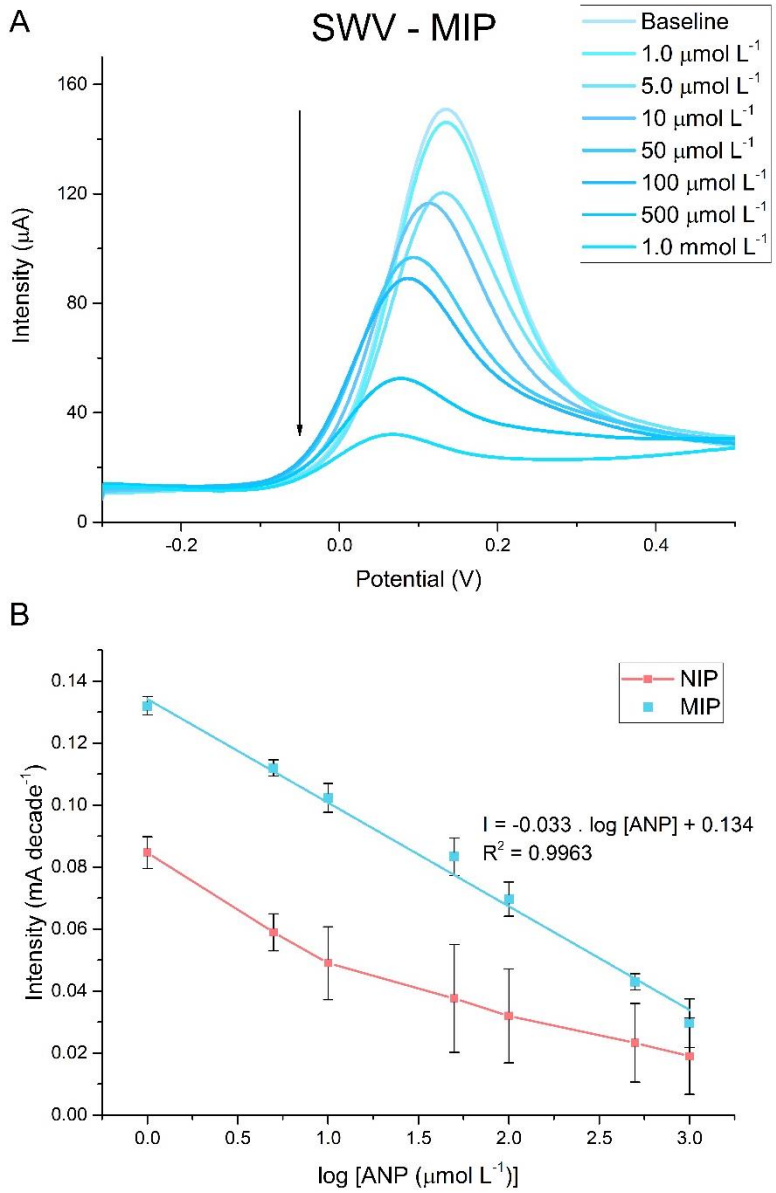

Figure 20 – Detection studies performed by evaluation of the developed MIP biosensor response to ANP standard solutions increasing concentration (1.0 µmol L^{-1} – 1.0 mmol L^{-1}). **A –** SWV measurements acquired for the different ANP standard solutions tested. Baseline – PB 0.1 mol L^{-1}, pH 7.2. **B –** Calibration curves obtained for the MIP (blue) and NIP (pink) biosensors. The experiments were performed in triplicate (n = 3).

To evaluate the reproducibility of the biosensor, three MIP films were prepared and used to perform the detection of ANP in different days. Based on the current intensity responses obtained, the respective coefficient of variation of the biosensor response for each ANP concentration tested was determined. Low values were obtained for almost all the concentrations (< 10%), characteristic of a good day-to-day reproducibility of the preparation of the MIP film receptor. In this work, the regeneration of the biosensor was

not tested, to prevent contamination between samples. The fact that this biosensor presents a low cost of production allows for it to be a disposable device for single use.

The recovery of the developed biosensor was also evaluated by comparing the real ANP concentration value in solution with the one reported by the MIP biosensor. For the two solutions tested, of concentration 5.0 μmol L^{-1} and 10 μmol L^{-1} of ANP, recovery values of 101 % and 105 % were obtained, respectively, which indicates a good recovery.

4.4.2. Adsorption isotherms

An adsorption isotherm describes the retention of a substance in solution (adsorbate) to a solid-phase (adsorbent), which can be a MIP film. When the solution containing the adsorbate is in contact with the adsorbent enough time, an adsorption equilibrium is achieved, with the remaining adsorbate present in the bulk solution being in a dynamic balance with the interface adsorbate concentration.[90]

There are various mathematical correlations presented over the years that provide insight into the adsorption mechanism of different systems.[90] Two of the most common models are the Langmuir and Freundlich isotherms, which are empirical models, based on different thermodynamic assumptions that generate characteristic curves characterized by their respective physicochemical parameters.

The Langmuir isotherm model follows 4 assumptions: (a) homogeneous and fixed number of adsorption sites; (b) monolayer adsorption; (c) no interaction between the adsorbed molecules and; (d) equal adsorption and desorption rates at equilibrium conditions.[90-92] In electrochemical studies, this isotherm can be represented mathematically by the following equation:

$$\frac{I_0 - I}{I_0} = \frac{Q_m . K_L . C}{1 + K_L . C} \quad \textbf{(4)}$$

where I_0 corresponds to the peak current before incubation with ANP (baseline), I is the peak current after incubation with the corresponding ANP concentration (C), Q_m is the maximum adsorption capacity and K_L corresponds to the Langmuir association constant.[91]

The Freundlich isotherm assumes a multilayer adsorption with heterogeneous sites, with non-uniform distribution of adsorption heat and affinities over the heterogeneous surface.[90, 91, 93]

For the electrochemical experiments developed in this work, this isotherm can be written as:

$$\frac{I_0 - I}{I_0} = K_F . C^{\frac{1}{n_F}} \quad \textbf{(5)}$$

Where n_F represents the surface heterogeneity or adsorption intensity and K_F corresponds to the Freundlich constant representing the adsorption capacity.[91]

The electrochemical data obtained (i.e. the SWV response of the biosensor for several ANP concentrations tested) was fitted to the Freundlich and Langmuir models, as shown in **Figure 21**. From these curves, the isotherm parameters, as well as the chi-square value of the mathematical fit obtained for each model were determined and summarized in **Table 3**.

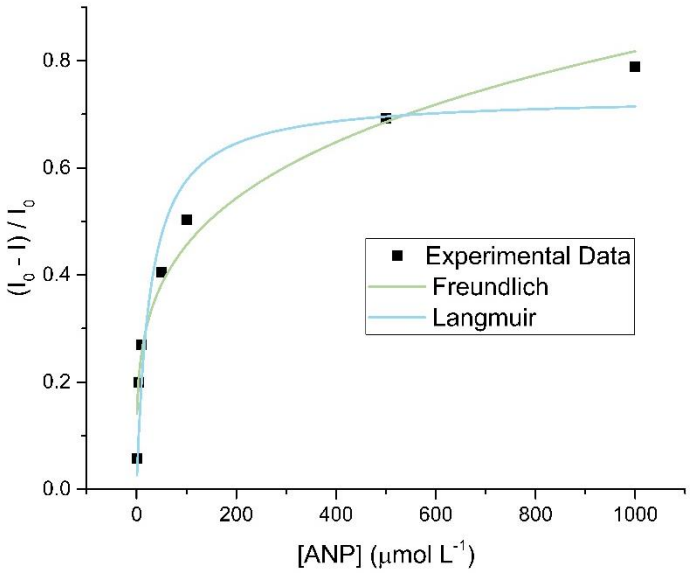

Figure 21 – Fitting of Freundlich and Langmuir adsorption isotherms to the experimental data obtained with the developed MIP biosensor.

Table 3 – Freundlich and Langmuir adsorption isotherms coefficients and chi-square obtained for the mathematical fit.

Freundlich			Langmuir		
K_F / L µmol^{-1}	1 / n_F	χ^2	K_L / L µmol^{-1}	Q_m	χ^2
0.14 ± 0.02	0.25 ± 0.03	0.0022	0.04 ± 0.02	0.73 ± 0.06	0.0059

To determine the model capable of best describing the interaction between the ANP molecule and the MIP constructed, the chi-square values (χ^2) obtained for each isotherm were compared. The χ^2 value is a statistic parameter that compares the difference between the theoretical values, obtained by the model, with the experimental values. Therefore, the lower the χ^2 value, the better model fitting.[94] Thus, in this work, the Freundlich isotherm model described better the interaction between ANP and the MIP film receptor surface. This agrees with literature, where, generally, Freundlich isotherm performs better in adsorption studies carried out at MIP films.[77, 95]

The dissociation constant (K_D) value of 7.1 µmol L^{-1} was calculated as the inverse of the binding constant determined using the Freundlich adsorption isotherm (K_F) and represents similar affinity to a polyclonal antibody (K_D around µmol L^{-1}). A similar dissociation constant of 7.9 µmol L^{-1} was obtained by Wang *et al.*[9], who synthesized MIP NPs for ANP detection.

According to the theory, when $1/n_F$ is between 0 and 1, the adsorption is considered favourable, being irreversible when it is equal to 1, and unfavourable when above it.[91] In this work, the $1/n_F$ value obtained (0.25 ± 0.03) (n_F = 3.93) allowed to affirm that the adsorption to the MIP system is favourable.

4.4.3. Selectivity studies

In this work, studies to evaluate the selectivity of the developed MIP biosensor were performed. The molecules selected as interferents for the study were:

(i) BSA (66.0 kDa), which in terms of size, is much larger when compared to ANP (size exclusion effect);
(ii) Vancomycin (1.49 kDa), whose size is lower than the target analyte in this work (size exclusion effect) and;
(iii) Myoglobin (18.0 kDa), which is a cardiac biomarker that can co-exist with the target analyte in biological samples.

After testing the developed MIP biosensor response against target and interferent solutions (concentration of 500 µmol L^{-1}) the results were represented as the difference between the SWV peak current intensity of baseline (I_0) and the molecule tested (I), as shown in **Figure 22**.

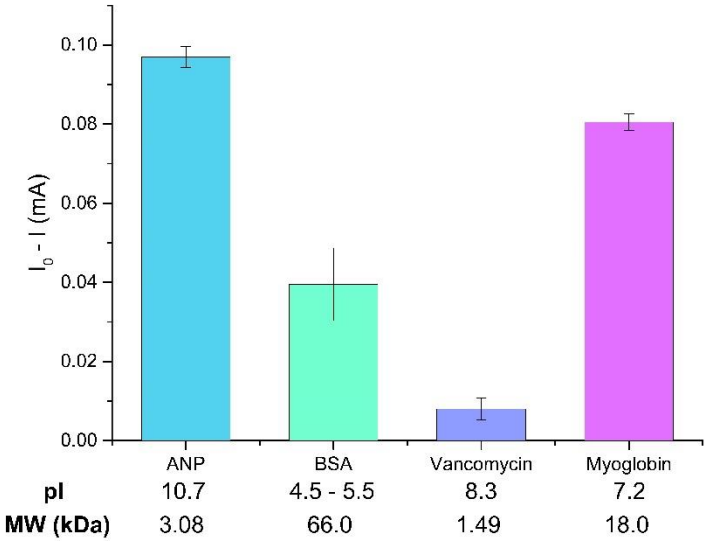

Figure 22 – Selectivity of the constructed biosensor by assessing the response to 500 µmol L^{-1} of ANP, BSA, vancomycin and myoglobin. Assays were performed at least in duplicate (n ≥ 2) Respective isoelectric point (pI) and molecular weight (MW, kDa) were included in the figure.

The developed biosensor showed considerable response to BSA when compared to ANP. Although BSA is known for its spontaneous adsorption to metal surfaces[96], being widely used as a surface blocking agent in various biosensing devices,[97] this scenario is unlikely for the MIP biosensor since all the gold working area is expected to be covered by the thin film. Thus, the biosensor response to BSA is probably due to its non-specific adsorption to the film at the biosensor surface. However, it is expected that the hydrophilic DA film had an important contribution to minimize this effect.

It is important to notice that polydopamine film presents zwitterionicity (pI = 3.4) because of the many amino and phenolic groups present in the polymeric chains. When pH < 3.4, polydopamine surface is charged positively due to the protonation of the amino groups. On the contrary, when pH > 3.4, polydopamine surface is negatively charged due to the deprotonation of the phenolic group present in the molecule.[49, 98] Thus, the electrostatic repulsion between polydopamine and BSA, which is also negatively charged, can contribute to minimize its non-specific adsorption to the MIP film.

Electrostatic repulsion is an important effect to take in account when the detection is performed with biological samples (e.g., human serum), because it can decrease not only the interference of albumin, but also other non-target molecules.[99] The effect of electrostatic repulsion can be potentiated by reducing the ionic strength of the medium, i.e., PB 0.1 mol L^{-1} to 0.01 mol L^{-1}.[100]

In relation to vancomycin, the low biosensor response can be explained by its smaller size when compared to ANP, leading to weak complementarity in size and shape between vancomycin and the binding sites. Also, the molecular structure of vancomycin is very different to the one of ANP, contributing for weak interactions in the binding sites present in the MIP film.

The biosensor response towards myoglobin was fairly similar to the one for ANP. In the pH value that these studies were performed, myoglobin presents no charge. Thus, in principle, no significant electrostatic repulsions occur between the myoglobin and the polydopamine film, favouring its non-specific adsorption to the MIP film. Besides, the post-modification of polydopamine films with proteins has been described in the literature. This occurs through the reaction of amino or thiol groups present in proteins with the catechol groups present in the polydopamine film, that become extremely reactive under slightly basic conditions.[53] This kind of reaction might happen between the amino groups of myoglobin and polydopamine, increasing its adsorption to the MIP film.

From the results obtained, myoglobin can be considered as an interferent for the detection of ANP in biological samples for cardiovascular diseases diagnosis. However, this effect could be minimized in detection studies by preparing the ANP solutions in a medium with higher pH value. At pH 8.0, for example, myoglobin might present a clear negative charge, while polydopamine maintains negatively charged, increasing the electrostatic repulsion. Still, myoglobin is not present in the ANP-nanoparticles samples tested in this work to evaluate the biosensor applicability.

4.5. Biosensor construction using epitope imprinting approach

The molecular imprinting of macromolecules, such as peptides and proteins, can be a challenge due to its complex and flexible structure and difficult extraction from the polymeric matrix.[65] Knowing this, the epitope imprinting approach was applied for the receptor film construction in this work, further identified as epitope MIP (EMIP). The ANP epitope chosen has the following aminoacid sequence: H_2N- cysteine; asparagine; serine; phenylalanine; arginine; tyrosine -COOH. A concentration of 0.5 mg mL^{-1} was used to perform the imprinting.

As can be seen in the voltammograms represented in **Figure 23-A**, the peak current intensity of the EMIP after extraction is similar to the peak current intensity after treating the NIP surface with the extraction solution, which means that the template extraction efficiency from the EMIP film was really low. Furthermore, the EMIP biosensor (**Figure 23-B**) showed a non-linear response to ANP and similar to the NIP response, meaning that, most likely, the interactions between the target analyte and the biosensor surface are predominantly non-specific. Thus, this implies that a non-successful imprinting process occurred during the EMIP construction, probably due to:

(i) the ANP epitope chosen as template. The aminoacid sequence of the epitope contains a terminal cysteine (with a -SH group). Thiols are commonly used in the biosensing field to create self-assembled monolayers (SAMs) on gold surfaces through the formation of a stable gold-sulphur covalent bond.[101, 102] Thus, in this work, probably the cysteine-terminal epitope present in the polymeric solution will rapidly covalently attach to the gold electrode surface, making the template extraction difficult. Therefore, almost no recognition sites were created during EMIP construction.

(ii) the low concentration of template epitope used for the EMIP construction, which leads to a scarce number of recognition sites present in the polymer film, limiting the biosensor interaction with the target analyte and making the biosensor prone to saturate.

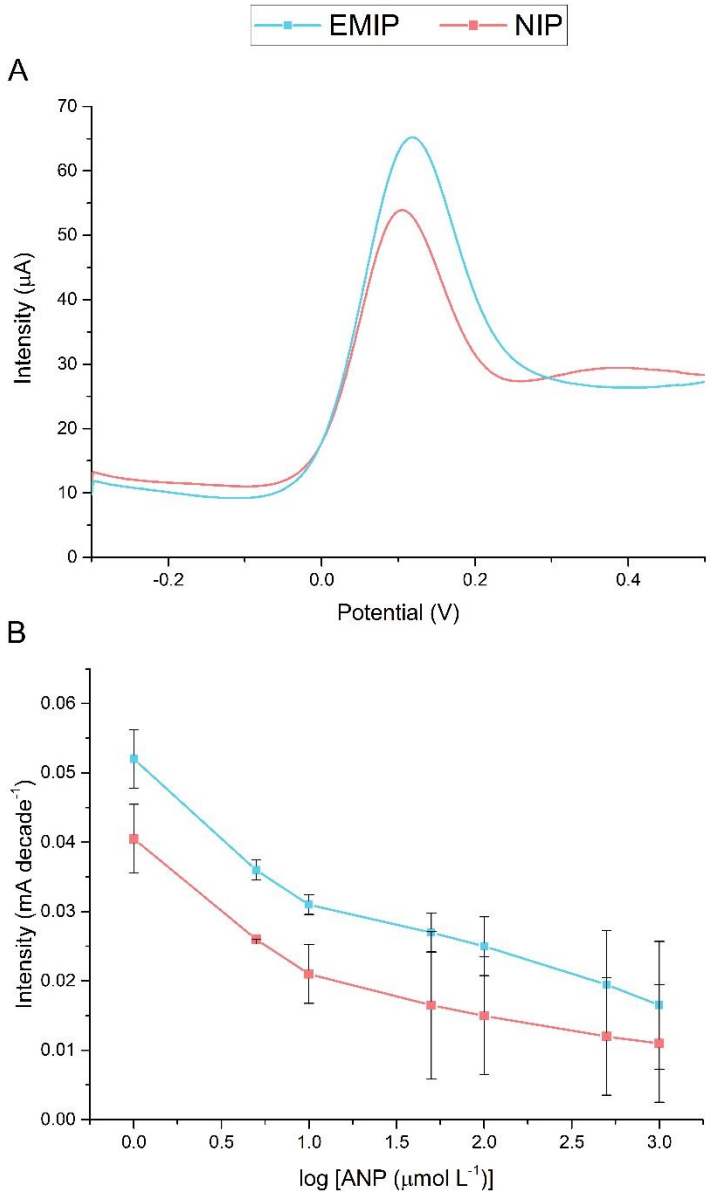

Figure 23 – Results obtained with the biosensor constructed using epitope imprinting approach (EMIP) (template 0.5 mg mL^{-1}). **A –** SWV voltammograms recorded after treating the EMIP (blue) and NIP (pink) surfaces with extraction solution. **B –** Calibration curves obtained for the EMIP (blue) and NIP (pink) biosensors. ANP standard solutions: 1.0 µmol L^{-1} – 1.0 mmol L^{-1}. Assays were performed in duplicate (n = 2).

4.6. Biosensor application for ANP-nanoparticles detection

As stated before, the biosensor described in this work was developed with the aim of detecting ANP coupled to NPs used to perform targeted drug delivery, allowing to understand the cellular internalization of the NPs.

Firstly, the PLGA NPs functionalized with ANP (PLGA-NPs@ANP) were tested using both the NIP and the MIP biosensor. To evaluate the molecular imprinting effect, the biosensor response to non-functionalized NPs (PLGA-NPs) was also studied, working as a reference system since it can only occur non-specific interactions. This last study also allowed to evaluate the selectivity that the functionalization with ANP confers to the drug-loaded NPs to natriuretic peptide receptors present in cardiac cells.

To study the biosensor response to NPs standard solutions with concentrations ranging from 4.0 μg mL^{-1} to 100.0 μg mL^{-1}, the same indirect method was used as before, that is to collect SWV voltammograms in the presence of the redox probe, 5 mM HCF, after 15 minutes of incubation of the AuSPE surface with the NPs solution. To obtain the calibration curves for the studied systems, the SWV peak current intensity was represented as a function of NPs concentration logarithm.

As can be seen in **Figure 24-A**, the prepared MIP biosensor presented a linear response to the PLGA-NPs@ANP which indicates that specific interactions between the ANP molecules on the NPs surface and the recognition sites at the polymer film are occurring. On the other end, the response of the NIP to the functionalized NPs was random.

In addition, to evaluate the selectivity that ANP brings to the synthesized NPs, the biosensor response to non-functionalized NPs was also studied (**Figure 24-B**). As expected, the biosensor only presented a linear response to the PLGA-NPs@ANP, which characterizes the specific interactions occurring between the ANP-nanoparticles and the imprinted cavities present in the synthetic receptor MIP film.

So, the developed MIP biosensor can not only detect ANP in its free form, in solution, but also attached to the surface of NPs.

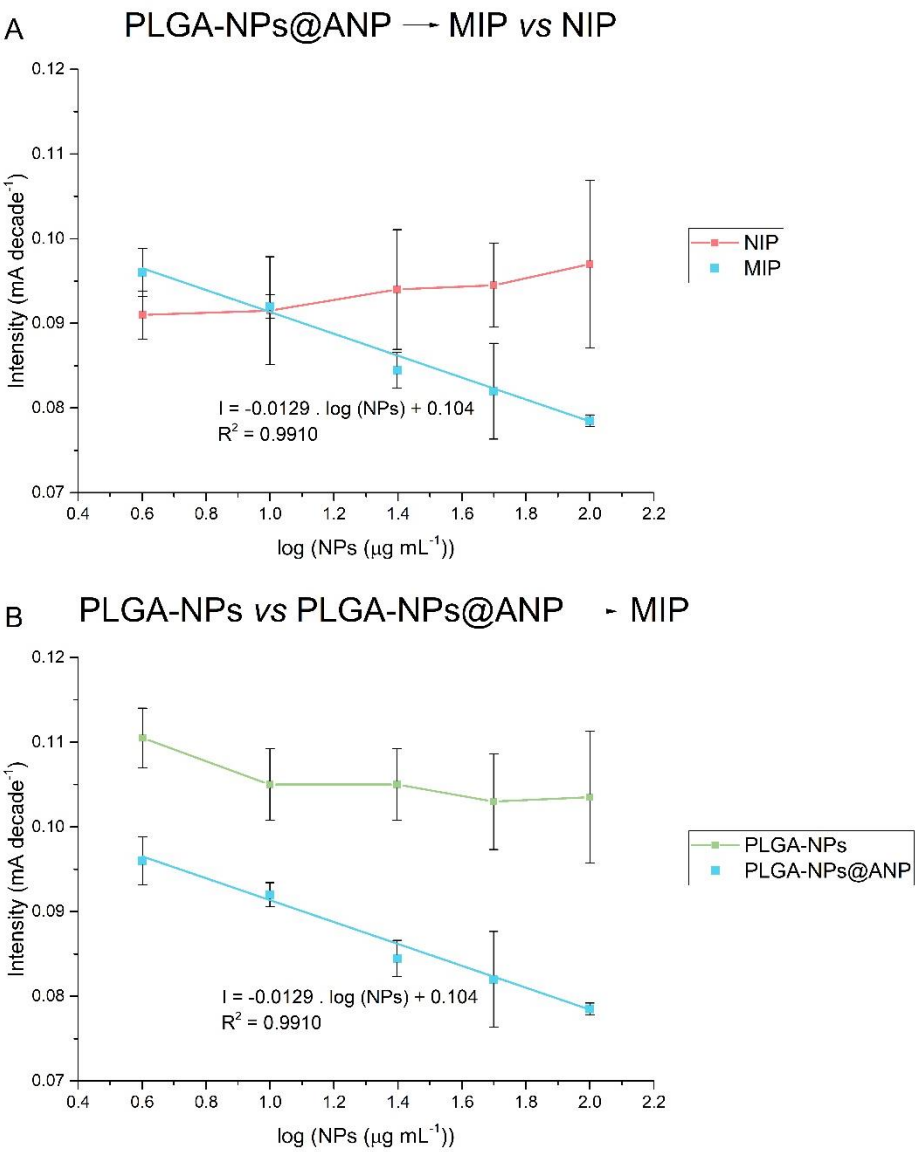

Figure 24 – Detection studies of the developed biosensor with standard solutions of non-functionalized PLGA-NPs and ANP functionalized PLGA-NPs (PLGA-NPs@ANP) (concentration ranging from 4.0 μg mL^{-1} to 200 μg mL^{-1}). **A –** Calibration curves for PLGA-NPs@ANP with the MIP (blue) and the NIP (pink). **B –** Calibration curves for the MIP with PLGA-NPs (green) and PLGA-NPs@ANP (blue). Assays were performed in duplicate (n = 2).

Although these are preliminary studies, the results obtained are very promising, demonstrating that MI technology can be coupled to electrochemical detection to monitor targeted drug delivery, *in vitro* or even *in vivo*, providing a cheap and simple alternative to the techniques based on fluorescence commonly employed in these studies.

5. Conclusions and future perspectives

The aim of this work was the development of an amperometric biosensor using a molecularly imprinted polymer (MIP) receptor film, prepared by electrochemical polymerization of dopamine (DA) for selective quantification of atrial natriuretic peptide (ANP), as both biomarker and therapeutic agent for cardiovascular diseases, in particular heart failure.

Gold screen-printed electrodes (AuSPEs) were selected as substrates for the detection due to its low-cost and possibility of large-scale production of the biosensor for commercialization. Furthermore, electrochemical devices as the one used in this work are increasingly smaller and compact, allowing for ANP detection at point-of-care (POC) or *in situ* at the local of study.

In this work, DA was chosen as monomer due to its high biocompatibility and the functional groups it contains, that allows for the establishment of molecular interactions for efficient recognition of the target analyte. The DA electropolymerization was performed by using cyclic voltammetry (CV) technique, where the number of scan cycles performed allowed to easily control the film thickness, in order to maximize the biosensor performance, and 6 CV cycles were chosen to perform electropolymerization.

To further enhance the MIP biosensor response, other experimental conditions for the MIP construction were optimized, namely the: template extraction procedure and the template concentration. An efficient MIP for recognition of ANP was achieved using acetate buffer 0.05 mol L^{-1}, pH 4.5, containing 5 % (w/v) SDS as extraction solution, overnight under gentle agitation. The optimal ANP template concentration was found to be 0.5 mg mL^{-1}.

Although in this work the molecular imprinting of the whole peptide was successfully achieved, the epitope imprinting approach was also attempted in this work to further increase the MIP affinity for ANP and minimize the difficulties encountered by the imprinting of whole proteins. However, the EMIP biosensor did not provide an acceptable response to ANP, due to the inefficient extraction of the epitope from the polymeric matrix. This probably occurred due to the ANP epitope chosen to use as template, as it presents a terminal cysteine (containing a -SH group), that rapidly adsorbs to the gold electrode surface through a strong covalent interaction that difficult its posterior removal from the polymeric matrix for the formation of recognition sites.

Electrochemical, atomic force microscopy (AFM) and scanning electron microscopy (SEM) characterizations were performed on the electrode surface to confirm the surface modification by the electropolymerized MIP film. An almost complete blockage of the electrode surface after electropolymerization is important to minimize the non-specific adsorption. The hydrophilic properties of polydopamine are important to minimize this adsorption, essential to perform ANP detection in biofluids. AFM and SEM results were in accordance, where a smoother electrode surface appears after electropolymerization of DA.

To evaluate the analytical performance of the developed MIP biosensor, detection studies were performed. A linear biosensor response to ANP standard solutions in phosphate buffer (PB) in the concentration range from 1.0 μmol L^{-1} to 1.0 mmol L^{-1} was observed, with an LOD value < 1.0 μmol L^{-1}. It is difficult to affirm if the developed biosensor could be applied in clinical contest due to ANP being a biomarker under evaluation, where no cut-off values are well-established in the literature. Parallel studies with a NIP surface were performed that allowed to obtain an imprinting factor (IF) of 2.1, characterizing the specific interactions occurring at the MIP film.

Selectivity studies of the developed biosensor towards possible interferents were performed, such as bovine serum albumin (BSA), vancomycin and myoglobin. The biosensor presented some selectivity problems to BSA and myoglobin, that can be improved by increasing the pH value and/or reducing the ionic strength of the medium used to perform the detection studies. In this context, the selectivity to these molecules is not relevant, as they are not present in the samples for the biosensor application for ANP-nanoparticles detection.

The experimental results obtained were fitted to the Freundlich adsorption isotherm model. This model defines the heterogeneity of the MIP film surface, which can be explained by a high degree of freedom of the template in solution interacting with the monomer, leading to different types of binding sites. A dissociation constant (K_D) value of 7.1 μmol L^{-1} was obtained for the MIP, which represents similar affinity to a polyclonal antibody. The epitope imprinting approach could be one of the strategies to increase the MIP affinity to similar values of monoclonal antibodies, in the nmol L^{-1} range.

Finally, the applicability of the developed biosensor was evaluated by testing its ability to discriminate non-functionalized PLGA nanoparticles (PLGA-NPs) and ANP-functionalized particles (PLGA-NPs@ANP). A distinction between the two systems could be observed and a linear biosensor response towards PLGA-NPs@ANP was obtained.

Although further studies still need to be performed, these results showed to be promising for the use of MIPs coupled to electrochemical detection to study systems created to perform targeted drug delivery, *in vitro*.

Thus, aligned with the aim of this work, the following future work should be performed, namely:

- Study the biosensor application for PLGA-NPs@ANP detection. Evaluate the response of the biosensor to real samples of nanoparticles from cell uptake studies. Compare the results obtained with the ones obtained by the reference technique, flow cytometry.
- Improve the affinity and the biosensor analytical performance using:
    i. Epitope imprinting approach. As stated in the literature overview, using an epitope instead of the whole protein as template for MIP construction is beneficial on the binding sites formation. In this work, problems with epitope chosen were encountered. The selection of another epitope without terminal cysteines (e.g. H_2N- asparagine; serine; phenylalanine; arginine; tyrosine -COOH), should decrease its adsorption to the gold surface and allow a good imprinting of the template, promoting site accessibility and enhance the sensor selectivity and sensitivity.
    ii. self-reporting MIPs. The electrochemical detection of non-electroactive analytes is generally performed using indirect measurements with an external redox probe as the one used in this work (5 mmol L^{-1} $[Fe(CN)_6]^{4-}$ /$[Fe(CN)_6]^{3-}$). This increases the workload and time due to the successive incubations and respective measurements. In recent years, various works have reported the development of self-reporting MIPs.[103, 104] The incorporation of a redox-active molecule in the MIP or the formation of a self-assembled monolayer (SAM) with a terminal redox-active molecule on an electrode surface prior to the MIP film deposition, can make the MIP self-reporting, in other words, it presents double function of molecular recognition and reporting unit. In this work, preliminary studies were performed to evaluate the possibility of synthesizing self-reporting MIPs. A SAM with a terminal redox-active molecule was deposited on the electrode surface and then the film of polydopamine was formed. Although promising results were obtained (**Figure 25**), further studies

need to be performed, to evaluate this possibility and compare the analytical performance with the developed biosensor presented in this work.

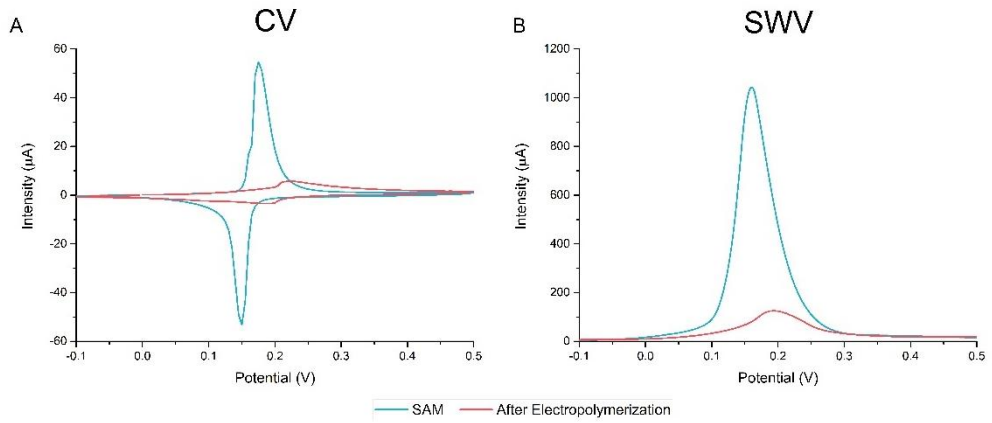

Figure 25 – Electrochemical characterization of a self-reporting MIP-biosensor after SAM formation (blue) and after electropolymerization (red). **A –** CV results. **B –** SWV results.

iii. nanoMIPs. The combination of molecular imprinting (MI) technology with nanotechnology has been emerging in the literature in recent years. Nanosized particles improves the binding sites accessibility, improving the template extraction paired with the increase of the number of imprinted cavities per unit of area. The incorporation of these materials as receptors in electrochemical biosensors have shown to improve its analytical performance when compared to MIP film layers.[14] Some work in this direction has already been developed in the research group.

Bibliography

(1) *Cardiovascular diseases (CVDs)*. World Health Organization, https://www.who.int/news-room/fact-sheets/detail/cardiovascular-diseases-(cvds) (accessed September 2023).

(2) Pollard, T. D.; Ong, J. J.; Goyanes, A.; Orlu, M.; Gaisford, S.; Elbadawi, M.; Basit, A. W. Electrochemical biosensors: a nexus for precision medicine. *Drug Discovery Today* **2021**, *26* (1), 69-79. DOI: https://doi.org/10.1016/j.drudis.2020.10.021.

(3) Mani, V.; Durmus, C.; Khushaim, W.; Ferreira, D. C.; Timur, S.; Arduini, F.; Salama, K. N. Multiplexed sensing techniques for cardiovascular disease biomarkers - A review. *Biosensors and Bioelectronics* **2022**, *216*, 114680. DOI: https://doi.org/10.1016/j.bios.2022.114680.

(4) Mansouri, S.; Oudah Mezan, S.; M. A. Altalbawy, F.; Kareem, A. K.; Rahi Alhachami, F.; Alexis Ramírez-Coronel, A.; Abdulfadhil Gatea, M.; Mireya Romero-Parra, R.; Fakri Mustafa, Y.; Hassan Jawhar, Z. Recent advances in assembly strategies of new advanced materials-based analytical methods for the detection of cardiac biomarkers as a diagnosis tool. *Microchemical Journal* **2023**, *191*, 108827. DOI: https://doi.org/10.1016/j.microc.2023.108827.

(5) Dhingra, R.; Vasan, R. S. Biomarkers in cardiovascular disease: Statistical assessment and section on key novel heart failure biomarkers. *Trends in Cardiovascular Medicine* **2017**, *27* (2), 123-133. DOI: https://doi.org/10.1016/j.tcm.2016.07.005.

(6) Katus, H. A.; Giannitsis, E. Biomarker in cardiology. *Clinical Research in Cardiology* **2018**, *107* (2), 10-15. DOI: 10.1007/s00392-018-1300-9.

(7) Nagai, C.; Minamino, N. Direct chemiluminescent enzyme immunoassay for atrial natriuretic peptide in mammalian plasma using a PEGylated antibody. *Analytical Biochemistry* **2014**, *461*, 10-16. DOI: https://doi.org/10.1016/j.ab.2014.05.022.

(8) Lin, C. Y.; Tsai, S. H.; Tai, D. F. Detection of oxytocin, atrial natriuretic peptide, and brain natriuretic peptide using novel imprinted polymers produced with amphiphilic monomers. *JOURNAL OF PEPTIDE SCIENCE* **2019**, *25* (3). DOI: 10.1002/psc.3150.

(9) Wang, C. Y.; Howell, M.; Raulji, P.; Davis, Y.; Mohapatra, S. Preparation and Characterization of Molecularly Imprinted Polymeric Nanoparticles for Atrial Natriuretic Peptide (ANP). *ADVANCED FUNCTIONAL MATERIALS* **2011**, *21* (23), 4423-4429. DOI: 10.1002/adfm.201100946.

(10) Torrieri, G.; Fontana, F.; Figueiredo, P.; Liu, Z.; Ferreira, M. P. A.; Talman, V.; Martins, J. P.; Fusciello, M.; Moslova, K.; Teesalu, T.; et al. Dual-peptide functionalized acetalated dextran-based nanoparticles for sequential targeting of macrophages during

myocardial infarction. *Nanoscale* **2020**, *12* (4), 2350-2358, 10.1039/C9NR09934D. DOI: 10.1039/C9NR09934D.

(11) Ferreira, M. P. A.; Ranjan, S.; Kinnunen, S.; Correia, A.; Talman, V.; Mäkilä, E.; Barrios-Lopez, B.; Kemell, M.; Balasubramanian, V.; Salonen, J.; et al. Drug-Loaded Multifunctional Nanoparticles Targeted to the Endocardial Layer of the Injured Heart Modulate Hypertrophic Signaling. *Small* **2017**, *13* (33), 1701276. DOI: https://doi.org/10.1002/smll.201701276 (acccessed 2023/09/10).

(12) Ferreira, M. P. A.; Talman, V.; Torrieri, G.; Liu, D. F.; Marques, G.; Moslova, K.; Liu, Z. H.; Pinto, J. F.; Hirvonen, J.; Ruskoaho, H.; et al. Dual-Drug Delivery Using Dextran-Functionalized Nanoparticles Targeting Cardiac Fibroblasts for Cellular Reprogramming. *ADVANCED FUNCTIONAL MATERIALS* **2018**, *28* (15). DOI: 10.1002/adfm.201705134.

(13) BelBruno, J. J. Molecularly Imprinted Polymers. *Chemical Reviews* **2019**, *119* (1), 94-119. DOI: 10.1021/acs.chemrev.8b00171.

(14) Silva, A. T.; Figueiredo, R.; Azenha, M.; Jorge, P. A. S.; Pereira, C. M.; Ribeiro, J. A. Imprinted Hydrogel Nanoparticles for Protein Biosensing: A Review. *ACS Sensors* **2023**, *8* (8), 2898-2920. DOI: 10.1021/acssensors.3c01010.

(15) Lee, C. Y. W.; Burnett, J. C. Natriuretic peptides and therapeutic applications. *Heart Failure Reviews* **2007**, *12* (2), 131-142. DOI: 10.1007/s10741-007-9016-3.

(16) Goetze, J. P.; Bruneau, B. G.; Ramos, H. R.; Ogawa, T.; de Bold, M. K.; de Bold, A. J. Cardiac natriuretic peptides. *Nature Reviews Cardiology* **2020**, *17* (11), 698-717. DOI: 10.1038/s41569-020-0381-0.

(17) Nagai-Okatani, C.; Kangawa, K.; Minamino, N. Three molecular forms of atrial natriuretic peptides: quantitative analysis and biological characterization. *JOURNAL OF PEPTIDE SCIENCE* **2017**, *23* (7-8), 486-495. DOI: 10.1002/psc.2969.

(18) Matsuo, A.; Nagai-Okatani, C.; Nishigori, M.; Kangawa, K.; Minamino, N. Natriuretic peptides in human heart: Novel insight into their molecular forms, functions, and diagnostic use. *Peptides* **2019**, *111*, 3-17. DOI: https://doi.org/10.1016/j.peptides.2018.08.006.

(19) Richards, A. M. The natriuretic peptides in heartfailure. *Basic Research in Cardiology* **2004**, *99* (2), 94-100. DOI: 10.1007/s00395-004-0461-z.

(20) de Bold, A. J.; Borenstein, H. B.; Veress, A. T.; Sonnenberg, H. A rapid and potent natriuretic response to intravenous injection of atrial myocardial extract in rats. *Life Sciences* **1981**, *28* (1), 89-94. DOI: https://doi.org/10.1016/0024-3205(81)90370-2.

(21) Kangawa, K.; Matsuo, H. Purification and complete amino acid sequence of α-human atrial natriuretic polypeptide (α-hANP). *Biochemical and Biophysical Research*

Communications **1984**, *118* (1), 131-139. DOI: https://doi.org/10.1016/0006-291X(84)91077-5.

(22) Song, W.; Wang, H.; Wu, Q. Atrial natriuretic peptide in cardiovascular biology and disease (NPPA). *Gene* **2015**, *569* (1), 1-6. DOI: https://doi.org/10.1016/j.gene.2015.06.029.

(23) Biomarkers and surrogate endpoints: Preferred definitions and conceptual framework. *Clinical Pharmacology & Therapeutics* **2001**, *69* (3), 89-95. DOI: https://doi.org/10.1067/mcp.2001.113989 (acccessed 2023/09/10).

(24) Yandle, T. G.; Richards, A. M.; Nicholls, M. G.; Cuneo, R.; Espiner, E. A.; Livesey, J. H. Metabolic clearance rate and plasma half life of alpha-human atrial natriuretic peptide in man. *Life Sciences* **1986**, *38* (20), 1827-1833. DOI: https://doi.org/10.1016/0024-3205(86)90137-2.

(25) Nakao, K.; Sugawara, A.; Morii, N.; Sakamoto, M.; Yamada, T.; Itoh, H.; Shiono, S.; Saito, Y.; Nishimura, K.; Ban, T.; et al. The pharmacokinetics ofα-human atrial natriuretic polypeptide in healthy subjects. *European Journal of Clinical Pharmacology* **1986**, *31* (1), 101-103. DOI: 10.1007/BF00870995.

(26) Michael, W.; Christian, H. Role of B-type natriuretic peptide (BNP) and NT-proBNP in clinical routine. *Heart* **2006**, *92* (6), 843. DOI: 10.1136/hrt.2005.071233.

(27) Semenov, A.; Katrukha, A. Analytical Issues with Natriuretic Peptides - has this been Overly Simplified? *EJIFCC* **2016**, *27*, 189-207.

(28) Senekovič Kojc, T.; Marčun Varda, N. Novel Biomarkers of Heart Failure in Pediatrics. In *Children*, 2022; Vol. 9.

(29) Gangnus, T.; Burckhardt, B. B. Potential and Limitations of Atrial Natriuretic Peptide as Biomarker in Pediatric Heart Failure—A Comparative Review. *Frontiers in Pediatrics* **2019**, *6*, Mini Review.

(30) Hulanicki, A.; Glab, S.; Ingman, F. Chemical sensors: definitions and classification. **1991**, *63* (9), 1247-1250. DOI: doi:10.1351/pac199163091247 (acccessed 2023-02-17).

(31) Thévenot, D. R.; Toth, K.; Durst, R. A.; Wilson, G. S. Electrochemical biosensors: recommended definitions and classification1International Union of Pure and Applied Chemistry: Physical Chemistry Division, Commission I.7 (Biophysical Chemistry); Analytical Chemistry Division, Commission V.5 (Electroanalytical Chemistry).1. *Biosensors and Bioelectronics* **2001**, *16* (1), 121-131. DOI: https://doi.org/10.1016/S0956-5663(01)00115-4.

(32) Bhalla, N.; Jolly, P.; Formisano, N.; Estrela, P. Introduction to biosensors. *Essays in Biochemistry* **2016**, *60* (1), 1-8. DOI: 10.1042/EBC20150001 (acccessed 9/11/2023).

(33) Garcia Cruz, A.; Haq, I.; Cowen, T.; Di Masi, S.; Trivedi, S.; Alanazi, K.; Piletska, E.; Mujahid, A.; Piletsky, S. A. Design and fabrication of a smart sensor using in silico epitope mapping and electro-responsive imprinted polymer nanoparticles for determination of insulin levels in human plasma. *Biosensors and Bioelectronics* **2020**, *169*, 112536. DOI: https://doi.org/10.1016/j.bios.2020.112536.

(34) de Lima, L. F.; Ferreira, A. L.; Awasthi, S.; Torres, M. D. T.; Friedman, H. M.; Cohen, G. H.; de Araujo, W. R.; de la Fuente-Nunez, C. Rapid and accurate detection of herpes simplex virus type 2 using a low-cost electrochemical biosensor. *Cell Reports Physical Science* **2023**, 101513. DOI: https://doi.org/10.1016/j.xcrp.2023.101513.

(35) Macovei, D.-G.; Irimes, M.-B.; Hosu, O.; Cristea, C.; Tertis, M. Point-of-care electrochemical testing of biomarkers involved in inflammatory and inflammatory-associated medical conditions. *Analytical and Bioanalytical Chemistry* **2023**, *415* (6), 1033-1063. DOI: 10.1007/s00216-022-04320-z.

(36) Karimi-Maleh, H.; Orooji, Y.; Karimi, F.; Alizadeh, M.; Baghayeri, M.; Rouhi, J.; Tajik, S.; Beitollahi, H.; Agarwal, S.; Gupta, V. K.; et al. A critical review on the use of potentiometric based biosensors for biomarkers detection. *Biosensors and Bioelectronics* **2021**, *184*, 113252. DOI: https://doi.org/10.1016/j.bios.2021.113252.

(37) Rebelo, P.; Costa-Rama, E.; Seguro, I.; Pacheco, J. G.; Nouws, H. P. A.; Cordeiro, M. N. D. S.; Delerue-Matos, C. Molecularly imprinted polymer-based electrochemical sensors for environmental analysis. *Biosensors and Bioelectronics* **2021**, *172*, 112719. DOI: https://doi.org/10.1016/j.bios.2020.112719.

(38) Mazzotta, E.; Di Giulio, T.; Malitesta, C. Electrochemical sensing of macromolecules based on molecularly imprinted polymers: challenges, successful strategies, and opportunities. *Analytical and Bioanalytical Chemistry* **2022**, *414* (18), 5165-5200. DOI: 10.1007/s00216-022-03981-0.

(39) Arduini, F. Electrochemical paper-based devices: When the simple replacement of the support to print ecodesigned electrodes radically improves the features of the electrochemical devices. *Current Opinion in Electrochemistry* **2022**, *35*, 101090. DOI: https://doi.org/10.1016/j.coelec.2022.101090.

(40) da Silva, E. T. S. G.; Souto, D. E. P.; Barragan, J. T. C.; de F. Giarola, J.; de Moraes, A. C. M.; Kubota, L. T. Electrochemical Biosensors in Point-of-Care Devices: Recent Advances and Future Trends. *ChemElectroChem* **2017**, *4* (4), 778-794. DOI: https://doi.org/10.1002/celc.201600758 (acccessed 2023/09/20).

(41) Wulff, G. Fourty years of molecular imprinting in synthetic polymers: origin, features and perspectives. *Microchimica Acta* **2013**, *180* (15), 1359-1370. DOI: 10.1007/s00604-013-0992-9.

(42) Akgönüllü, S.; Kılıç, S.; Esen, C.; Denizli, A. Molecularly Imprinted Polymer-Based Sensors for Protein Detection. In *Polymers*, 2023; Vol. 15.

(43) Guerreiro, A. R.; Chianella, I.; Piletska, E.; Whitcombe, M. J.; Piletsky, S. A. Selection of imprinted nanoparticles by affinity chromatography. *Biosensors and Bioelectronics* **2009**, *24* (8), 2740-2743. DOI: https://doi.org/10.1016/j.bios.2009.01.013.

(44) Kang, M. S.; Cho, E.; Choi, H. E.; Amri, C.; Lee, J.-H.; Kim, K. S. Molecularly imprinted polymers (MIPs): emerging biomaterials for cancer theragnostic applications. *Biomaterials Research* **2023**, *27* (1), 45. DOI: 10.1186/s40824-023-00388-5.

(45) He, J.-Y.; Li, Q.; Xu, H.-X.; Zheng, Q.-Y.; Zhang, Q.-H.; Zhou, L.-D.; Wang, C.-Z.; Yuan, C.-S. Recognition and analysis of biomarkers in tumor microenvironments based on promising molecular imprinting strategies with high selectivity. *TrAC Trends in Analytical Chemistry* **2023**, *162*, 117033. DOI: https://doi.org/10.1016/j.trac.2023.117033.

(46) Ben Moussa, F. Molecularly imprinted polymers meet electrochemical cancer chemosensors: A critical review from a clinical and economic perspective. *Microchemical Journal* **2023**, *191*, 108838. DOI: https://doi.org/10.1016/j.microc.2023.108838.

(47) Moreira Gonçalves, L. Electropolymerized molecularly imprinted polymers: perceptions based on recent literature for soon-to-be world-class scientists. *Current Opinion in Electrochemistry* **2021**, *25*, 100640. DOI: https://doi.org/10.1016/j.coelec.2020.09.007.

(48) Jamieson, O.; Betlem, K.; Mansouri, N.; Crapnell, R. D.; Vieira, F. S.; Hudson, A.; Banks, C. E.; Liauw, C. M.; Gruber, J.; Zubko, M.; et al. Electropolymerised molecularly imprinted polymers for the heat-transfer based detection of microorganisms: A proof-of-concept study using yeast. *Thermal Science and Engineering Progress* **2021**, *24*, 100956. DOI: https://doi.org/10.1016/j.tsep.2021.100956.

(49) Liu, Q.; Yu, B.; Ye, W.; Zhou, F. Highly Selective Uptake and Release of Charged Molecules by pH-Responsive Polydopamine Microcapsules. *Macromolecular Bioscience* **2011**, *11* (9), 1227-1234. DOI: https://doi.org/10.1002/mabi.201100061 (acccessed 2023/09/04).

(50) Li, S.; Wang, H.; Young, M.; Xu, F.; Cheng, G.; Cong, H. Properties of Electropolymerized Dopamine and Its Analogues. *Langmuir* **2019**, *35* (5), 1119-1125. DOI: 10.1021/acs.langmuir.8b01444.

(51) Lee, H.; Dellatore, S. M.; Miller, W. M.; Messersmith, P. B. Mussel-Inspired Surface Chemistry for Multifunctional Coatings. *Science* **2007**, *318* (5849), 426-430. DOI: 10.1126/science.1147241 (acccessed 2023/09/13).

(52) Ryu, J. H.; Messersmith, P. B.; Lee, H. Polydopamine Surface Chemistry: A Decade of Discovery. *ACS Applied Materials & Interfaces* **2018**, *10* (9), 7523-7540. DOI: 10.1021/acsami.7b19865.

(53) Lynge, M. E.; van der Westen, R.; Postma, A.; Städler, B. Polydopamine—a nature-inspired polymer coating for biomedical science. *Nanoscale* **2011**, *3* (12), 4916-4928, 10.1039/C1NR10969C. DOI: 10.1039/C1NR10969C.

(54) Cai, S.; Cheng, Y.; Qiu, C.; Liu, G.; Chu, C. The versatile applications of polydopamine in regenerative medicine: Progress and challenges. *Smart Materials in Medicine* **2023**, *4*, 294-312. DOI: https://doi.org/10.1016/j.smaim.2022.11.005.

(55) Szewczyk, J.; Aguilar-Ferrer, D.; Coy, E. Polydopamine films: Electrochemical growth and sensing applications. *European Polymer Journal* **2022**, *174*, 111346. DOI: https://doi.org/10.1016/j.eurpolymj.2022.111346.

(56) Bisht, N.; Dwivedi, N.; Khosla, A.; Mondal, D. P.; Srivastava, A. K.; Dhand, C. Review—Recent Advances in Polydopamine-based Electrochemical Biosensors. *Journal of The Electrochemical Society* **2022**, *169* (10), 107505. DOI: 10.1149/1945-7111/ac9b95.

(57) Qi, J.; Li, B.; Zhou, N.; Wang, X.; Deng, D.; Luo, L.; Chen, L. The strategy of antibody-free biomarker analysis by in-situ synthesized molecularly imprinted polymers on movable valve paper-based device. *Biosensors and Bioelectronics* **2019**, *142*, 111533. DOI: https://doi.org/10.1016/j.bios.2019.111533.

(58) Leibl, N.; Duma, L.; Gonzato, C.; Haupt, K. Polydopamine-based molecularly imprinted thin films for electro-chemical sensing of nitro-explosives in aqueous solutions. *Bioelectrochemistry* **2020**, *135*, 107541. DOI: https://doi.org/10.1016/j.bioelechem.2020.107541.

(59) Roushani, M.; Zalpour, N. Selective detection of Asulam with in-situ dopamine electropolymerization based electrochemical MIP sensor. *Reactive and Functional Polymers* **2021**, *169*, 105069. DOI: https://doi.org/10.1016/j.reactfunctpolym.2021.105069.

(60) Karimian, N.; Turner, A. P. F.; Tiwari, A. Electrochemical evaluation of troponin T imprinted polymer receptor. *Biosensors and Bioelectronics* **2014**, *59*, 160-165. DOI: https://doi.org/10.1016/j.bios.2014.03.013.

(61) Mabrouk, M.; Hammad, S. F.; Abdella, A. A.; Mansour, F. R. Tips and tricks for successful preparation of molecularly imprinted polymers for analytical applications: A critical review. *Microchemical Journal* **2023**, *193*, 109152. DOI: https://doi.org/10.1016/j.microc.2023.109152.

(62) Yarman, A.; Jetzschmann, K. J.; Neumann, B.; Zhang, X.; Wollenberger, U.; Cordin, A.; Haupt, K.; Scheller, F. W. Enzymes as Tools in MIP-Sensors. In *Chemosensors*, 2017; Vol. 5.

(63) Sharma, P. S.; Garcia-Cruz, A.; Cieplak, M.; Noworyta, K. R.; Kutner, W. 'Gate effect' in molecularly imprinted polymers: the current state of understanding. *Current Opinion in Electrochemistry* **2019**, *16*, 50-56. DOI: https://doi.org/10.1016/j.coelec.2019.04.020.

(64) Zahedi, P.; Ziaee, M.; Abdouss, M.; Farazin, A.; Mizaikoff, B. Biomacromolecule template-based molecularly imprinted polymers with an emphasis on their synthesis strategies: a review. *Polymers for Advanced Technologies* **2016**, *27* (9), 1124-1142. DOI: https://doi.org/10.1002/pat.3754 (acccessed 2023/09/20).

(65) Yang, K.; Li, S.; Liu, L.; Chen, Y.; Zhou, W.; Pei, J.; Liang, Z.; Zhang, L.; Zhang, Y. Epitope Imprinting Technology: Progress, Applications, and Perspectives toward Artificial Antibodies. *Advanced Materials* **2019**, *31* (50), 1902048, https://doi.org/10.1002/adma.201902048. DOI: https://doi.org/10.1002/adma.201902048 (acccessed 2023/02/13).

(66) Teixeira, S. P. B.; Reis, R. L.; Peppas, N. A.; Gomes, M. E.; Domingues, R. M. A. Epitope-imprinted polymers: Design principles of synthetic binding partners for natural biomacromolecules. *Science Advances 7* (44), eabi9884. DOI: 10.1126/sciadv.abi9884 (acccessed 2023/02/13).

(67) Bard, A. J.; Faulkner, L. R. *Electrochemical Methods: Fundamentals and Applications*; Wiley, 2000.

(68) Elgrishi, N.; Rountree, K. J.; McCarthy, B. D.; Rountree, E. S.; Eisenhart, T. T.; Dempsey, J. L. A Practical Beginner's Guide to Cyclic Voltammetry. *Journal of Chemical Education* **2018**, *95* (2), 197-206. DOI: 10.1021/acs.jchemed.7b00361.

(69) Mabbott, G. A. An introduction to cyclic voltammetry. *Journal of Chemical Education* **1983**, *60* (9), 697. DOI: 10.1021/ed060p697.

(70) Forster, R. J.; Walsh, D. A. VOLTAMMETRY | Overview. In *Encyclopedia of Analytical Science (Second Edition)*, Worsfold, P., Townshend, A., Poole, C. Eds.; Elsevier, 2005; pp 181-188.

(71) Simões, F. R.; Xavier, M. G. 6 - Electrochemical Sensors. In *Nanoscience and its Applications*, Da Róz, A. L., Ferreira, M., de Lima Leite, F., Oliveira, O. N. Eds.; William Andrew Publishing, 2017; pp 155-178.

(72) Fischer, L.; Tenje, M.; Heiskanen, A.; Masuda, N.; Castillo, J.; Bentien, A.; Emnéus, J.; Jakobsen, M.; Boisen, A. Gold cleaning methods for electrochemical detection applications. *Microelectronic Engineering* **2009**, *86*, 1282-1285.

(73) Kounaves, S. P. *Handbook of Instrumental Techniques for Analytical Chemistry*; 1998.

(74) Ribeiro, J. A. Caraterização e Otimização de Sensores Eletroquímicos para Aminas Biogénicas. Thesis to obtain the doctoral degree in Chemistry. Faculty of Sciences of the University of Portoo, 2013.

(75) O'Dea, J. J.; Osteryoung, J.; Osteryoung, R. A. Theory of square wave voltammetry for kinetic systems. *Analytical Chemistry* **1981**, *53* (4), 695-701. DOI: 10.1021/ac00227a028.

(76) Aoki, K.; Tokuda, K.; Matsuda, H.; Osteryoung, J. Reversible square-wave voltammograms independence of electrode geometry. *Journal of Electroanalytical Chemistry and Interfacial Electrochemistry* **1986**, *207* (1), 25-39. DOI: https://doi.org/10.1016/0022-0728(86)87060-7.

(77) Ribeiro, J.; Pereira, C.; Silva, A. F.; Sales, M. G. Electrochemical detection of cardiac biomarker myoglobin using polyphenol as imprinted polymer receptor. *Analytica Chimica Acta* **2017**, *981*. DOI: 10.1016/j.aca.2017.05.017.

(78) Wang, Y.; Han, M.; Ye, X.; Wu, K.; Wu, T.; Li, C. Voltammetric myoglobin sensor based on a glassy carbon electrode modified with a composite film consisting of carbon nanotubes and a molecularly imprinted polymerized ionic liquid. *Microchimica Acta* **2017**, *184* (1), 195-202. DOI: 10.1007/s00604-016-2005-2.

(79) Buck, R. P.; Lindner, E. Recommendations for nomenclature of ionselective electrodes (IUPAC Recommendations 1994). **1994**, *66* (12), 2527-2536. DOI: doi:10.1351/pac199466122527 (acccessed 2023-06-27).

(80) Wang, J.-l.; Li, B.-c.; Li, Z.-j.; Ren, K.-f.; Jin, L.-j.; Zhang, S.-m.; Chang, H.; Sun, Y.-x.; Ji, J. Electropolymerization of dopamine for surface modification of complex-shaped cardiovascular stents. *Biomaterials* **2014**, *35* (27), 7679-7689. DOI: https://doi.org/10.1016/j.biomaterials.2014.05.047.

(81) Li, Y.; Liu, M.; Xiang, C.; Xie, Q.; Yao, S. Electrochemical quartz crystal microbalance study on growth and property of the polymer deposit at gold electrodes during oxidation of dopamine in aqueous solutions. *Thin Solid Films* **2006**, *497* (1), 270-278. DOI: https://doi.org/10.1016/j.tsf.2005.10.048.

(82) Leibl, N.; Haupt, K.; Gonzato, C.; Duma, L. Molecularly Imprinted Polymers for Chemical Sensing: A Tutorial Review. In *Chemosensors*, 2021; Vol. 9.

(83) Kruk, T.; Bzowska, M.; Hinz, A.; Szuwarzyński, M.; Szczepanowicz, K. Control of Specific/Nonspecific Protein Adsorption: Functionalization of Polyelectrolyte Multilayer Films as a Potential Coating for Biosensors. In *Materials*, 2021; Vol. 14.

(84) De Middeleer, G.; Dubruel, P.; De Saeger, S. Characterization of MIP and MIP functionalized surfaces: Current state-of-the-art. *TrAC Trends in Analytical Chemistry* **2016**, *76*, 71-85. DOI: https://doi.org/10.1016/j.trac.2015.11.007.

(85) Butterworth, A.; Blues, E.; Williamson, P.; Cardona, M.; Gray, L.; Corrigan, D. K. SAM Composition and Electrode Roughness Affect Performance of a DNA Biosensor for Antibiotic Resistance. In *Biosensors*, 2019; Vol. 9.

(86) Rebelo, T. S. C. R.; Miranda, I. M.; Brandão, A. T. S. C.; Sousa, L. I. G.; Ribeiro, J. A.; Silva, A. F.; Pereira, C. M. A Disposable Saliva Electrochemical MIP-Based Biosensor for Detection of the Stress Biomarker α-Amylase in Point-of-Care Applications. In *Electrochem*, 2021; Vol. 2, pp 427-438.

(87) Zamani, M.; Yang, V.; Maziashvili, L.; Fan, G.; Klapperich, C. M.; Furst, A. L. Surface Requirements for Optimal Biosensing with Disposable Gold Electrodes. *ACS Measurement Science Au* **2022**, *2* (2), 91-95. DOI: 10.1021/acsmeasuresciau.1c00042.

(88) *Atrial Natriuretic Peptide (ANP) Competitive ELISA Kit*. https://www.thermofisher.com/elisa/product/Atrial-Natriuretic-Peptide-ANP-Competitive-ELISA-Kit/EIAANP (accessed 19/09/2023).

(89) Erdem, Ö.; Eş, I.; Saylan, Y.; Atabay, M.; Gungen, M. A.; Ölmez, K.; Denizli, A.; Inci, F. In situ synthesis and dynamic simulation of molecularly imprinted polymeric nanoparticles on a micro-reactor system. *Nature Communications* **2023**, *14* (1), 4840. DOI: 10.1038/s41467-023-40413-8.

(90) Foo, K. Y.; Hameed, B. Insights into Modeling of Adsorption Isotherm Systems. *Chemical Engineering Journal* **2010**, *156*, 2-10. DOI: 10.1016/j.cej.2009.09.013.

(91) Kalam, S.; Abu-Khamsin, S. A.; Kamal, M. S.; Patil, S. Surfactant Adsorption Isotherms: A Review. *ACS Omega* **2021**, *6* (48), 32342-32348. DOI: 10.1021/acsomega.1c04661.

(92) Langmuir, I. THE CONSTITUTION AND FUNDAMENTAL PROPERTIES OF SOLIDS AND LIQUIDS. PART I. SOLIDS. *Journal of the American Chemical Society* **1916**, *38* (11), 2221-2295. DOI: 10.1021/ja02268a002.

(93) Al-Ghouti, M. A.; Da'ana, D. A. Guidelines for the use and interpretation of adsorption isotherm models: A review. *Journal of Hazardous Materials* **2020**, *393*, 122383. DOI: https://doi.org/10.1016/j.jhazmat.2020.122383.

(94) Alavi, M.; Visentin, D. C.; Thapa, D. K.; Hunt, G. E.; Watson, R.; Cleary, M. Chi-square for model fit in confirmatory factor analysis. *Journal of Advanced Nursing* **2020**, *76* (9), 2209-2211, https://doi.org/10.1111/jan.14399. DOI: https://doi.org/10.1111/jan.14399 (acccessed 2023/07/20).

(95) Yazdani, Z.; Yadegari, H.; Heli, H. A molecularly imprinted electrochemical nanobiosensor for prostate specific antigen determination. *Analytical Biochemistry* **2019**, *566*, 116-125. DOI: https://doi.org/10.1016/j.ab.2018.11.020.

(96) Zhang, X.; Yarman, A.; Erdossy, J.; Katz, S.; Zebger, I.; Jetzschmann, K. J.; Altintas, Z.; Wollenberger, U.; Gyurcsányi, R. E.; Scheller, F. W. Electrosynthesized MIPs for transferrin: Plastibodies or nano-filters? *Biosensors and Bioelectronics* **2018**, *105*, 29-35. DOI: https://doi.org/10.1016/j.bios.2018.01.011.

(97) Wang, R.; Zhou, X.; Zhu, X.; Yang, C.; Liu, L.; Shi, H. Isoelectric Bovine Serum Albumin: Robust Blocking Agent for Enhanced Performance in Optical-Fiber Based DNA Sensing. *ACS Sensors* **2017**, *2* (2), 257-262. DOI: 10.1021/acssensors.6b00746.

(98) Ouyang, Z.; Huang, Z.; Tang, X.; Xiong, C.; Tang, M.; Lu, Y. A dually charged nanofiltration membrane by pH-responsive polydopamine for pharmaceuticals and personal care products removal. *Separation and Purification Technology* **2019**, *211*, 90-97. DOI: https://doi.org/10.1016/j.seppur.2018.09.059.

(99) Bernsmann, F.; Frisch, B.; Ringwald, C.; Ball, V. Protein adsorption on dopamine–melanin films: Role of electrostatic interactions inferred from ζ-potential measurements versus chemisorption. *Journal of Colloid and Interface Science* **2010**, *344* (1), 54-60. DOI: https://doi.org/10.1016/j.jcis.2009.12.052.

(100) Winkler, K.; Paszewski, M.; Kalwarczyk, T.; Kalwarczyk, E.; Wojciechowski, T.; Gorecka, E.; Pociecha, D.; Holyst, R.; Fialkowski, M. Ionic Strength-Controlled Deposition of Charged Nanoparticles on a Solid Substrate. *The Journal of Physical Chemistry C* **2011**, *115*, 19096-19103. DOI: 10.1021/jp206704s.

(101) Bürgi, T. Properties of the gold–sulphur interface: from self-assembled monolayers to clusters. *Nanoscale* **2015**, *7* (38), 15553-15567, 10.1039/C5NR03497C. DOI: 10.1039/C5NR03497C.

(102) Rouhana, L. L.; Moussallem, M. D.; Schlenoff, J. B. Adsorption of Short-Chain Thiols and Disulfides onto Gold under Defined Mass Transport Conditions: Coverage, Kinetics, and Mechanism. *Journal of the American Chemical Society* **2011**, *133* (40), 16080-16091. DOI: 10.1021/ja2041833.

(103) Rebocho, S.; Cordas, C. M.; Viveiros, R.; Casimiro, T. Development of a ferrocenyl-based MIP in supercritical carbon dioxide: Towards an electrochemical sensor for bisphenol A. *The Journal of Supercritical Fluids* **2018**, *135*, 98-104. DOI: https://doi.org/10.1016/j.supflu.2018.01.006.

(104) Lach, P.; Cieplak, M.; Noworyta, K. R.; Pieta, P.; Lisowski, W.; Kalecki, J.; Chitta, R.; D'Souza, F.; Kutner, W.; Sharma, P. S. Self-reporting molecularly imprinted polymer with the covalently immobilized ferrocene redox probe for selective electrochemical

sensing of p-synephrine. *Sensors and Actuators B: Chemical* **2021**, *344*, 130276. DOI: https://doi.org/10.1016/j.snb.2021.130276.

Annex 1

Annex 1 – Stability of DA solution along the time

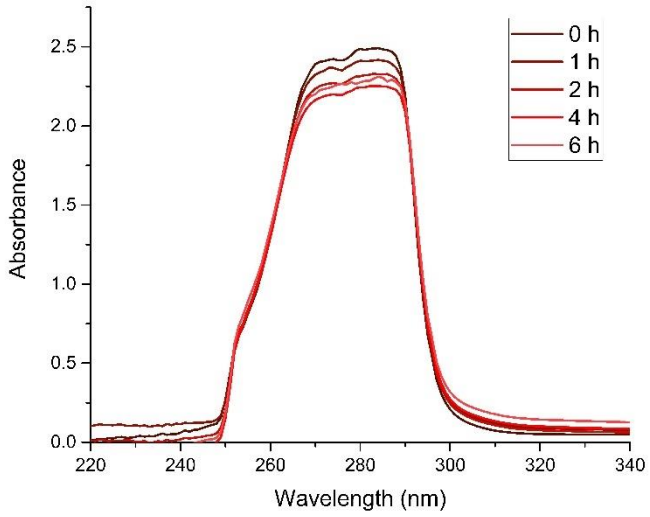

Figure 26 - UV-Vis spectrum of dopamine solution (8 mmol L^{-1}) in PB 0.1 mol L^{-1}, pH 7.2, to evaluate its stability along the time.

Annex 2

Annex 2 – Representative CV curve of the electropolymerization of DA in the presence of ANP

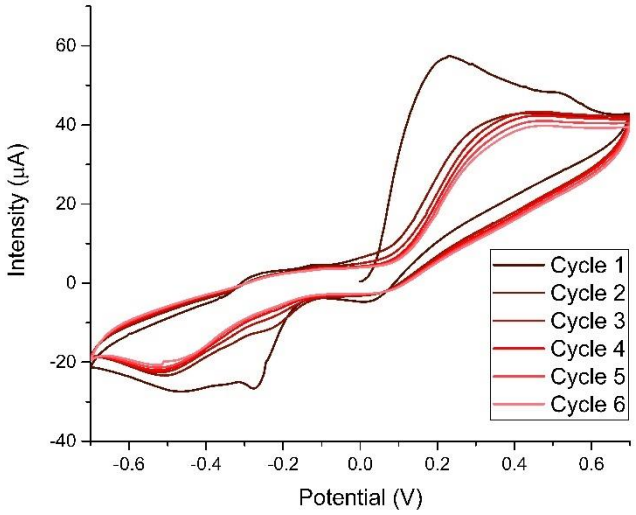

Figure 27 - Electropolymerization of dopamine solution (2 mmol L^{-1}) in the presence of the template molecule (ANP 0.5 mg mL^{-1}) during 6 CV cycles. The scan rate was 50 mV s^{-1}.